GEOLOGICA CARPATHICA, FEBRUARY 2022, 73, 1, 25–42 https://doi.org/10.31577/GeolCarp.73.1.2

Provenance of the Lower Cretaceous clastic rocks from the Gadvan Formation (Zagros Basin, Iran): Evidences from whole-rock geochemistry and petrography

FATEMEH RAMEZANI[1], MAHBOUBEH HOSSEINI-BARZI[2,✉], JAVAD HONARMAND[3], ABBAS SADEGHI[4] and JOHN S. ARMSTRONG-ALTRIN[5]

[1]Shahid Beheshti University, Faculty of Earth Science, Iran; fa_ramezani@sbu.ac.ir
[2]Shahid Beheshti University, Faculty of Earth Science, Iran; ✉m_hosseini@sbu.ac.ir
[3]Research Institute of Petroleum Industry, Iran; honarmandj@gmail.com
[4]Shahid Beheshti University, Faculty of Earth Science, Iran; A-Sadeghi@sbu.ac.ir
[5]Universidad Nacional Autónoma de México, Instituto de Ciencias del Mar y Limnología, Unidad de Procesos Oceánicos y Costeros, Ciudad Universitaria, Ciudad de México 04510, México; armstrong@cmarl.unam.mx

(Manuscript received July 5, 2021; accepted in revised form January 4, 2022; Associate Editor: Katarína Bónová)

Abstract: The petrography and geochemistry of clastic rocks from the Gadvan Formation in the Abadan Plain (southwest Iran) were analysed to infer their weathering intensity, compositional maturity, provenance, and tectonic setting. The Index of Compositional Variability (0.47–0.71) indicates high compositional and mineralogical maturity. The Chemical Index of Alteration and the Plagioclase Index of Alteration suggest high intensity of chemical weathering in the source area. In addition, a remarkable high content of REE and LREE/HREE and Th/U ratios, as well as high C-value (1.7) suggest high chemical weathering in the source area. Rounded zircon grains, mineral homogeneity, and a lack of feldspar grains could be related to high weathering and the effect of recycling. Elemental ratios (La/Sc, La/Co, Th/Sc, Th/Co, Gd_N/Yb_N, Cr/Ni, Co/Th, La/Yb, and La/Th), bivariate diagrams (La/Sc vs. Co/Th, La/Sc vs. Th/Co, Cr/Th vs. Th/Sc, Th/Yb vs. Ta/Yb, and La/ Yb vs. La/Th), and an enrichment of Nb, Zr, Th, La, Cr, Ni contents imply felsic to intermediate parent rocks, which are similar to the massive granitoids of the Arabian Shield. This could be supported by the dominance of zircon grains, as well as inclusions of rutile and tourmaline in quartz grains in the Gadvan sandstones. Moreover, further petrographical evidences, such as undulatory quartz grains, rare biotite and a small orientation of grains is also related to low-grade metamorphism in a felsic source rock. Finally, the Mudrock Maturity Index and tectonic discrimination diagrams reveal a convergence process in a collisional setting, in which the Zagros Mountains originated.

Keywords: provenance, tectonic setting, paleoweathering, Gadvan Formation, Abadan Plain, Zagros Basin.

Introduction

As a part of the Khami Group (Fahliyan, Gadvan, Dariyan Formations), the Lower Cretaceous Gadvan Formation in the Abadan Plain comprises siliciclastic rocks, such as sandstone, siltstone and shale/claystone. The overlying and underlying rock units of the Gadvan Formation are Fahliyan and Dariyan Formations in the type section, as well as in the Abadan Plain. The Gadvan Formation is equivalent to the Zubair Formation in Iraq and Kuwait, the Biyadh Formation in Saudi Arabia, the Kharaib Formation in Qatar, Oman, and the United Arab Emirates (Sharland et al. 2001). The Gadvan Formation has a different name in the south-east Iraq (Zubair Formation) with the same lithology and the same name in the Dezful Embayment, Ize Zone, and Fars Province; however, with different lithology (carbonate). This formation is 200–300 m thick (the area of Abadan Plain is 26,500 km^2) and its type section, which is located at the eastern end of Kuh-e Gadvan (42 km east-north-east of Shiraz), consists of gray and green to brownish yellow marl or shale, and dark gray argillaceous limestone (Motiei 1993).

The geochemistry of siliciclastic rocks is widely used in various studies to infer the tectonic setting and provenance (e.g., Taylor & McLennan 1985; Roser & Korsch 1988; Cox et al. 1995; Heins & Kairo 2007; Etemad-Saeed et al. 2011, 2015; Armstrong-Altrin et al. 2012, 2014, 2015; Armstrong-Altrin 2015). The ratio of the most immobile elements increases towards a passive margin due to the relative tectonic stability and prolonged weathering (Zimmermann & Bahlburg 2003; Armstrong-Altrin et al. 2004). These ratios can be recorded in sediments as an indicator of paleoclimatic changes and the degree of sediment recycling (Nesbitt & Young 1982; Chittleborough 1991). Therefore, major, trace, and rare earth element (REE) geochemistry of siliciclastic rocks is considered a good indicator for tracing variables, such as parent rock, weathering, oxic and anoxic conditions, as well as tectonic setting (Ravnas & Furnes 1995; Nath et al. 1997; Getaneh 2002; Dobrzinski et al. 2004; LaMaskin et al. 2008; Etemad-Saeed et al. 2011; Shadan & Hosseini-Barzi 2013; Jafarzadeh et al. 2014; Etemad-Saeed et al. 2015; Mir 2015; Mir et al. 2016; Ngueutchoua et al. 2017; Gazi et al. 2017; Khazaei et al. 2018).

Some important questions still exist concerning the Gadvan Formation, such as: Where is the source of sediments? What is the composition of its source rocks? What type of tectonic setting is dominant in the source area? And what was the weathering condition like during deposition? In order to answer these questions, we analysed the petrography and geochemistry of fine-grained siliciclastic rocks from the Gadvan Formation in the Abadan Plain (southwest Iran). The aim of this study is to infer the weathering, provenance, and tectonic setting of the Gadvan Formation in the Lower Cretaceous of the Zagros Basin.

Geological setting

The Abadan Plain is a structural zone located between the Arabian Plate to the south-west and the Zagros Fold-Thrust Belt (ZFTB) to the north-east (Alavi 2004; McQuarrie 2004) (Fig. 1). Hence, the geological and structural features, as well as the evolution of this zone are influenced by both of them, mostly by the Arabian Plate (Aqrawi & Badics 2015; Assadi et al. 2016). During the late Permian to mid-Cenomanian, extension between the Sanandaj–Sirjan and central Iran terranes (northwest Iran, Alborz, and Lut blocks) led to the creation of the Neo-Tethys Ocean as well as a passive margin in the north-east part of the Arabian Plate margin (Sharland et al. 2001; Piryaei et al. 2010). Progressive uplift of the western plate area commenced in the Early Cretaceous, possibly as a result of the opening of the South and Central Atlantic Ocean (Condie 1989; Sharland et al. 2001). These major tectonic events changed the northeastward tilt of the plate to an eastward tilt and were responsible for driving a major clastic sediment load in the deltaic system of the Zubair Formation from the western parts of the plate (in Iraq and Kuwait) (Loosveld et al. 1996; Al-Fares et al. 1998) to its distal equivalent, the Gadvan Formation fine deposits in Iran (Motiei 1993). After the mid-Cenomanian, the Neo-Tethys Ocean began to close and caused subduction of the oceanic crust beneath the central Iranian plate (Sharland et al. 2001; Sepehr & Cosgrove 2004; Alavi 2007; Heydari 2008; Piryaei et al. 2010, 2011). The Gadvan Formation siliciclastic sediments in the Abadan Plain were supplied from the above-mentioned sedimentary systems, which preserved all of the tectonic and sedimentary events.

Materials and methods

In total, 350 mudrock and sandstone samples were selected from a core at different intervals of 4 wells (A, B, E, D) of the Gadvan Formation in the Abadan Plain (Figs. 1 and 2). The sandstones were studied in terms of their texture, fabric,

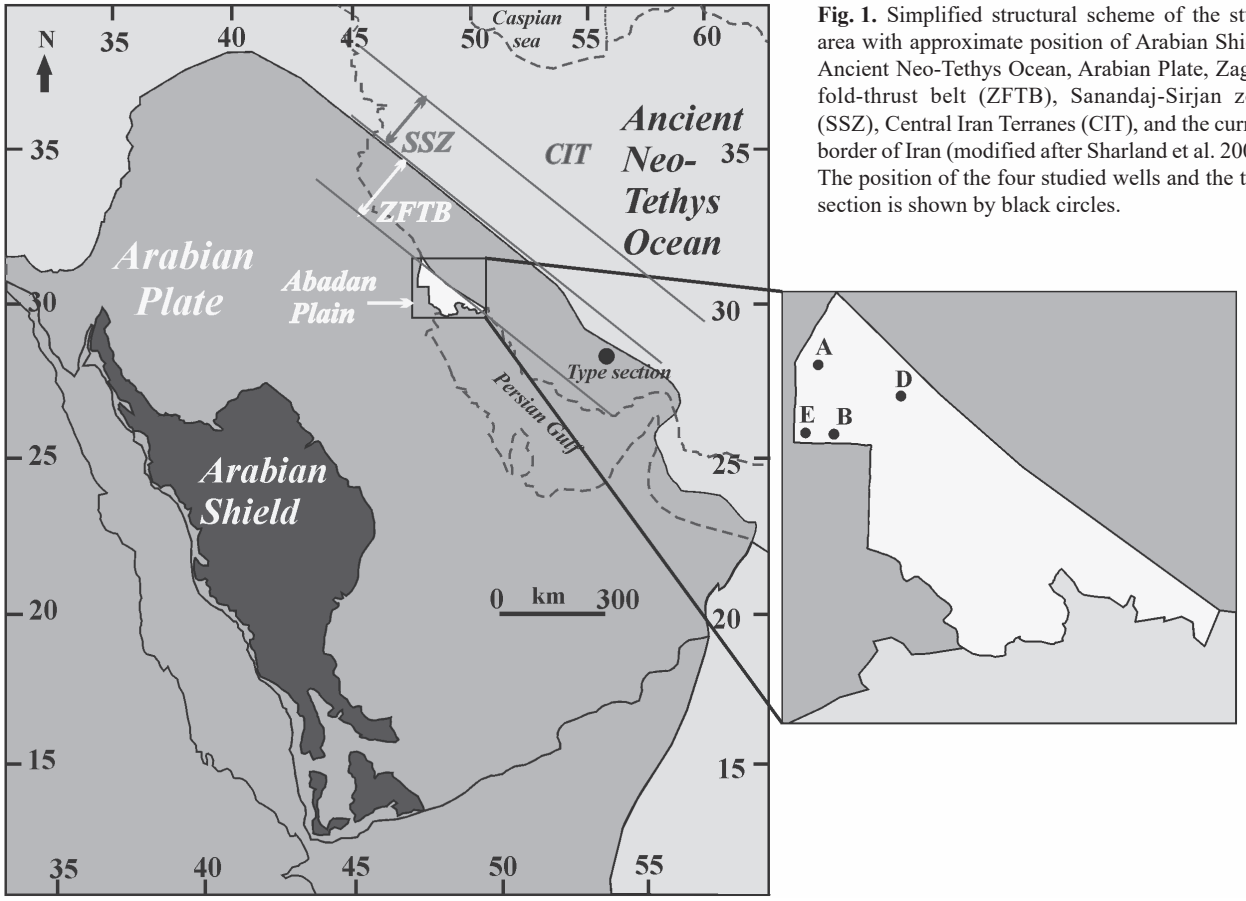

Fig. 1. Simplified structural scheme of the study area with approximate position of Arabian Shield, Ancient Neo-Tethys Ocean, Arabian Plate, Zagros fold-thrust belt (ZFTB), Sanandaj-Sirjan zone (SSZ), Central Iran Terranes (CIT), and the current border of Iran (modified after Sharland et al. 2001). The position of the four studied wells and the type section is shown by black circles.

and composition by optical microscopy. After performing calcimetery of 37 mudrock samples by a Bernard calcimeter, 31 mudstone samples were selected for geochemical analysis (Fig. 2), taking into consideration the lowest $CaCO_3$ content (<5 % $CaCO_3$; Pettijohn 1975).

The mineralogical composition of 15 fine-grained mudrocks of the Gadvan Formation was investigated using a PHILIPS (PW1800) X-ray (XRD) in the mineralogical laboratories of the Kansaran binaloud company of Iran. Based on the protocol developed by Tucker (1988), bulk powder of samples was prepared by removing carbonate and organic matter (using H_2O_2 and acetic acid) (Kunze & Dixon 1986). Afterwards, it was treated by cation saturation, ethylene glycol saturation, and heat treatment (to 350 °C initially, and then 550 °C) (Hardy & Tucker 1988). Identification and semi-quantitative evaluation of the phases were performed using X'pert software (e.g., Backman et al. 2006). The obtained semi-quantitative percentages of the rock forming minerals and clay size fractions of the studied samples are presented in Table 1. The results of this analysis were used as a link between mudrock composition and the tectonic setting of the sedimentary basin (Mudrock Maturity Index: MMI) (Bhatia 1985). MMI is defined as 100 [phyllosilicates/(phyllosilicates+quartz+feldspars)] and MMI<33 represents tectic, 33–67 phyllo-tectic, and >68 phyllic mudrocks.

Fourteen bulk samples were powdered and their major element concentrations were analysed by X-ray fluorescence (XRF) spectrometry on fused beads (Rollinson 1993) at the Kansaran binaloud laboratories. The results are listed in Table 2. In addition, 31 samples were crushed into chips of 2–4 mm, cleaned in distilled water, dried, and then pulverized to a powder of 200 mesh in a tungsten carbide mill. Fused samples were diluted and analysed by Inductively Coupled Plasma–Mass Spectrometry (ICP–MS) (Perkin Elmer Sciex ELAN 6000, 6100 or 9000) at Actlabs in Ontario, Canada. These results are reported in Tables 3 and 4. We did not report the modal analysis data of the sandstones, due to their very fine to fine grain size. Petrographical evidences from these fine-grained sandstones were used for comparison with other results.

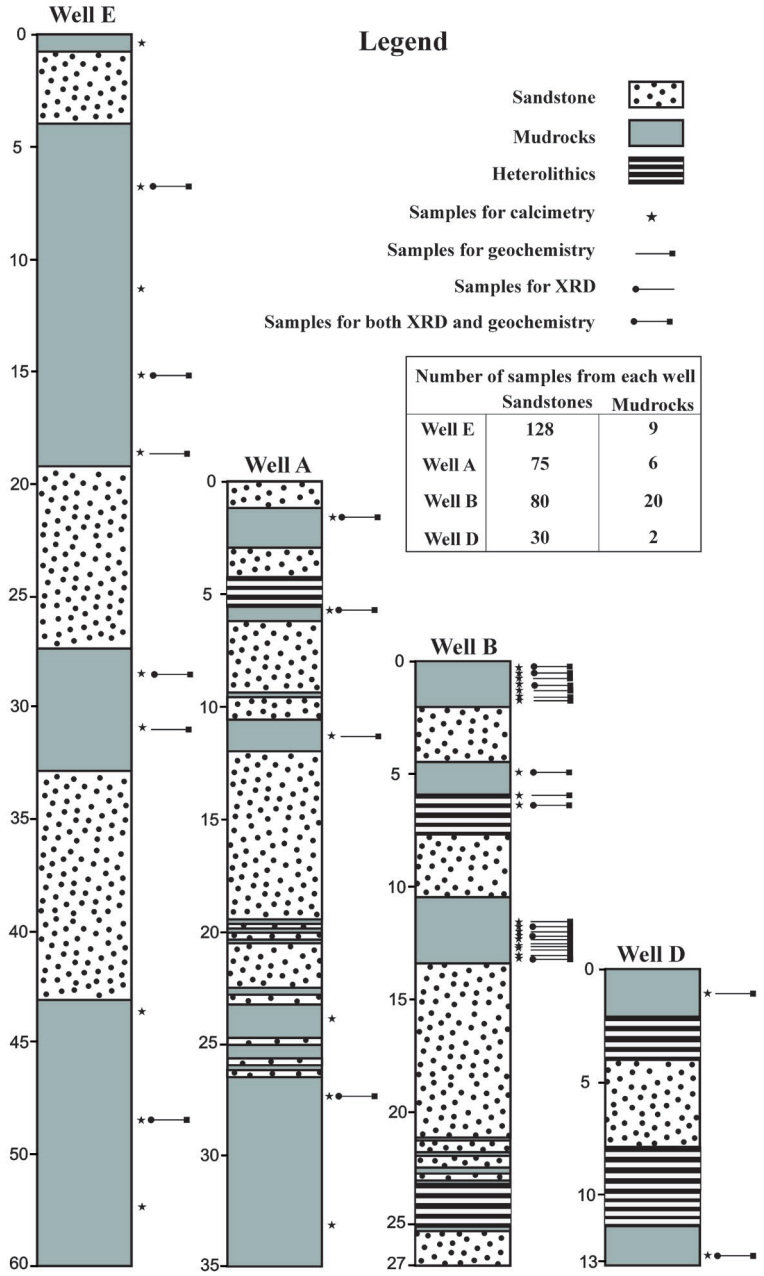

Fig. 2. The Gadvan Formation lithological column and location of the samples, which were selected from the four wells in the Abadan Plain (thickness in meters).

Results

Petrography

The Gadvan Formation in the Abadan Plain consists of very fine to fine-grained sandstones and mudrocks. Texturally, these grains are sub-rounded to rounded, poorly to well-sorted (bimodal inversion textures). The dominant framework constituent of the Gadvan sandstones is the monocrystalline quartz grains (Fig. 3A and B) with sub-equant shape and concave–convex contacts, and non-undulatory to slightly undulatory extinction. Polycrystalline quartz grains, which have up to 4 units per grain, show straight to slightly undulose extinction (Fig. 3B). Feldspars are not common and only a few orthoclases were observed in the thin sections. The dominant heavy minerals in the Gadvan sandstones are zircon (Fig. 4A and F), tourmaline (Fig. 4E and F), rutile (as a separate grain or inclusions in the monocrystalline quartz grains) (Fig. 4D

Table 1: XRD results of the Gadvan mudrocks, together with MMI classification from Bhatia (1985).

Sample No.	Quartz %	Feldspar (Alb. %)	Calcite %	Pyrite %	Heavy mineral %	Kaolinite %	Illite %	Chlorite %	SUM*	*MMI %* *(Mudrock Maturity Index)*	
G.A.P.2	40	5	1.5	2	<1.5	38	8	0	96	50.55	Phyllo-tectic
G.A.P.3	40	3	<1	9	1.5	36	7	0	97.5	50.00	Phyllo-tectic
G.A.P.5	42	0	2	6.5	<1.5	41	5	0	98	52.27	Phyllo-tectic
G.A.P.7	30	4	0	1	<1.5	49	11	0	96.5	63.83	Phyllo-tectic
G.A.P.9	34	5	1	1.5	1	45	9	0	96.5	58.06	Phyllo-tectic
G.A.P.14	30	5	0	2	1.5	48	12	0	98.5	63.16	Phyllo-tectic
G.A.P.16	29	5	0	4	<1.5	44	11	0	94.5	61.80	Phyllo-tectic
G.A.P.18	39	4	0	2	1.5	42	9	0	97.5	54.26	Phyllo-tectic
G.A.P.20	34	4	0	2	<1.5	45	10	0	96.5	59.14	Phyllo-tectic
G.A.P.29	36	4	0	4	1.5	37	15	0	97.5	56.52	Phyllo-tectic
G.A.P.31	35	4	1	1.5	1.5	45	8	0	96	57.61	Phyllo-tectic
G.A.P.33	39	5	1	2	1	40	8	0	96	52.17	Phyllo-tectic
G.A.P.34	32	2	0	3	<1.5	49	9	0	96.5	63.04	Phyllo-tectic
G.A.P.36	35	3	1	1	<1.5	43	6	3	93.5	57.78	Phyllo-tectic
G.A.P.37	30	4	3	1	<2	50	6	0	96	62.22	Phyllo-tectic

*The remnant of the constituents are not separable and therefore are not presented as percentage.

Table 2: XRF results of the Gadvan mudrocks.

Sample No.	SiO_2	Al_2O_3	Fe_2O_3	CaO	Na_2O	K_2O	MgO	TiO_2	MnO	P_2O_5	LOI	S ppm	CIA	PIA
G.A.P.2	49.84	24.84	5.57	1.07	0.47	2.1	1.36	1.72	0.03	0.068	12.72	1764	87	90.01
G.A.P.3	52.2	22.62	5.81	0.8	0.24	1.57	0.62	1.68	0.026	0.057	13.49	1231	90	95.29
G.A.P.4	47.25	24.01	8.72	0.32	0.49	1.63	1.25	1.43	0.042	0.073	0.775	14.07	88	96.45
G.A.P.6	49.12	23.65	8.26	0.64	0.57	1.92	2.42	1.33	0.034	0.083	0.889	10.97	87	93.65
G.A.P.7	43.82	23.75	8.19	3.75	0.36	1.38	2.01	1.56	0.05	0.135	1.326	13.77	87	94.13
G.A.P.9	51.01	24.73	6.25	0.87	0.53	2.24	1.34	1.47	0.041	0.075	11.33	1027	91	97.37
G.A.P.10	44.42	26.85	9.23	0.68	0.32	1.12	1.19	1.44	0.049	0.096	0.925	13.41	87	93.40
G.A.P.14	53.1	24.7	5.71	0.3	0.51	2.68	1.12	1.48	0.023	0.091	10.02	1425	91	97.17
G.A.P.18	52.39	25.58	5.86	0.22	0.42	1.87	1.23	1.63	0.014	0.081	10.52	1442	91	97.40
G.A.P.20	51.12	25.25	6.48	0.28	0.34	1.98	1.2	1.66	0.031	0.082	11.43	1386	90	97.69
G.A.P.29	46.97	28.88	5.67	0.22	0.4	2.61	1.29	1.54	0.017	0.089	12.19	1752	91	96.51
G.A.P.33	49.81	25.39	6.45	1.03	0.61	2.17	1.4	1.32	0.012	0.148	11.5	1973	93	96.26
G.A.P.34	52.14	23.88	6.87	0.29	0.35	1.84	1.22	1.70	0.023	0.077	11.45	1667	81	84.48
G.A.P.37	49.91	24.51	6.48	2.24	0.36	1.09	1.32	1.84	0.039	0.098	11.47	1044	88	94.72

and F) and opaque minerals. The pore spaces between grains are predominantly filled with rounded and multiple generation quartz overgrowths (Fig. 4B and C). Due to the very fine to fine-grained homogeneous nature of these sandstones, modal analysis could not be performed. Based on a percentage estimation comparison chart by Folk et al. (1970), these sandstones are classified as quartz arenite. The most important and primary evidences of parent rock mineralogy can be found in the detrital particles in siliciclastic rocks (Boggs 2009). Therefore, petrographic evidences from the sandstones were employed to infer the provenance and sedimentary recycling of the studied samples.

In general, the Gadvan mudrocks (Fig. 3C–F) are fossiliferous, massive (mudstone/silty mudstone/siltstone) to laminated (shale/marl) with different amounts of organic matter. The Gadvan mudrocks are predominantly composed of quartz, feldspar, calcite, pyrite, kaolinite, illite, and heavy minerals (Table 1). Moreover, MMI in the Gadvan mudrock samples is 50–63, which is classified as phyllo-tectic mudrocks (Table 1).

Geochemistry

Major element concentrations

The SiO_2 contents of the studied mudrock samples range from 43.82 to 53.1 wt. % with an average of 49.5, and Al_2O_3 contents vary from 22.62 to 28.88 wt. % with an average of 24.9 (Table 2). The average SiO_2/Al_2O_3 ratio (1.98) of these sediments is lower than that of the upper continental crust (UCC ~4.34; Taylor & McLennan 1985). TiO_2 values vary considerably (1.84–1.32 wt. %, average 1.55), while the Fe_2O_3 contents in these samples range between 5.57 and 9.23 wt. % with an average of 6.82 and the majority of the samples lying within the range of 1.42–1.55 wt. % for TiO_2 and 5.6–6.55 wt. % for Fe_2O_3, respectively. CaO and MgO range from 0.22–3.75 wt. % (average 0.91) and from 0.62–2.42 wt. % (average 1.36), respectively. K_2O contents (1.09–2.68 wt. %, average 1.87) are higher than those of Na_2O (0.24–0.61 wt. %, average 0.42). P_2O_5 and MnO contents are very low, ranging

Table 3: Trace and rare earth element concentrations (ppm) of the studied samples from the Gadvan Formation.

Sample No.	Ba	Ce	Co	Cr	Dy	Er	Eu	Gd	Ho	La	Lu	Nb	Nd	Ni	Pr	Rb	Sc	Sm	Sr	Tb	Th	Tm	U	V	Yb	Zr
G.A.P.2	3.2	141	11.6	124	5.72	3.29	1.76	7.23	1.12	77.8	0.41	40	52.5	26	20.4	75.2	22	9.08	184	1.02	20	0.47	3.37	155	2.9	203
G.A.P.3	3	123	12.5	105	4.83	2.87	1.29	5.56	0.98	67.7	0.39	38.1	41.2	28	12.1	54.3	19	6.76	190	0.82	19.8	0.43	3.04	148	2.66	204
G.A.P.5	3.3	135	10.8	97	5.61	2.76	1.91	8.01	1.01	71.9	0.33	38.1	52.1	25	19.5	34.7	16	10.1	210	1.08	29	0.38	2.83	108	2.38	184
G.A.P.7	2.8	122	13.7	122	4.59	2.39	1.59	6.36	0.85	64.9	0.28	29.9	45.5	31	12.6	75.2	22	7.98	174	0.85	16.1	0.33	2.44	169	2.04	131
G.A.P.8	2.8	119	13.7	117	4.72	2.69	1.48	5.82	0.91	64.8	0.33	30.2	43.4	31	12.2	75.8	19	7.42	156	0.84	17	0.38	2.56	150	2.33	143
G.A.P.9	2.9	114	14.4	106	4.71	2.27	1.41	5.55	0.92	62.4	0.34	30.3	42.2	32	11.9	74.9	20	7.1	156	0.8	16.6	0.39	2.36	151	2.38	153
G.A.P.10	2.4	143	15.4	97	12.3	4.45	5.53	20.8	1.96	69.9	0.46	19.8	82.2	29	23.5	65.9	21	25.4	207	2.83	15	0.57	2.49	164	3.36	166
G.A.P.11	2.7	98.7	18.7	124	4.69	2.8	1.35	5.49	0.95	59.2	0.38	31.3	35.8	33	9.77	74.3	22	6.63	165	0.8	14	0.42	2.38	182	2.65	194
G.A.P.12	2.7	98.7	18	127	4.66	2.8	1.31	5.36	0.95	58.7	0.39	31.9	36.1	33	9.82	72.4	22	6.58	174	0.79	14	0.41	2.37	191	2.61	190
G.A.P.13	2.7	92.6	18.3	127	4.12	2.49	1.09	4.52	0.86	54.6	0.36	32	32.8	34	9.18	64.8	20	5.47	166	0.67	13.2	0.38	2.28	192	2.4	189
G.A.P.14	4.7	76.4	16.6	119	3.76	2.4	0.87	3.9	0.78	48.1	0.33	36.9	26.3	27	7.48	67.9	16	4.49	156	0.59	10.3	0.36	2.99	170	2.23	223
G.A.P.15	4	144	19.9	92	9.89	4.72	3.27	13.8	1.8	85.2	0.57	34	64.5	30	21.7	71.5	16	16	183	1.99	16.1	0.67	3.65	140	4.01	229
G.A.P.16	4.2	148	19.2	140	6.53	3.97	1.9	8.06	1.34	88.5	0.57	36.1	54.2	31	20.2	62.7	17	9.86	180	1.11	17.4	0.63	3.51	236	4.14	229
G.A.P.17	3.2	105	13.4	91	4.48	2.49	1.2	5.19	0.87	61.3	0.35	37.2	37.5	27	10.4	47.8	15	6.54	166	0.76	14.9	0.4	2.86	117	2.32	236
G.A.P.18	3.3	110	13.4	91	4.58	2.5	1.22	5.29	0.86	64.2	0.34	38.3	39.1	27	10.7	51.5	15	6.59	170	0.75	15.6	0.37	2.84	122	2.26	229
G.A.P.19	3.3	140	17.7	109	5.89	3.14	1.78	7.37	1.13	82.3	0.43	41.7	50.1	34	13.8	61.7	17	9.1	187	1.07	20.2	0.46	3.23	154	2.89	234
G.A.P.20	3.4	151	17	105	5.82	3.35	1.6	6.82	1.16	88.4	0.44	41.5	52.3	32	20.1	67.7	20	8.51	195	0.96	30.8	0.49	3.04	155	3.02	234
G.A.P.21	3.5	136	17.3	103	5.26	3.03	1.44	6.09	1.04	79.6	0.41	41.2	47.8	34	13.4	63.9	17	7.8	195	0.87	19.6	0.44	3.45	153	2.79	229
G.A.P.22	3.5	168	19.9	111	9.25	4.33	3.34	13.9	1.64	95	0.48	43.3	71.9	38	24.5	67.1	20	16.5	221	1.88	32.9	0.57	3.32	177	3.4	232
G.A.P.23	3.5	111	16	109	4.82	2.67	1.39	5.83	0.94	65.7	0.36	42.5	40.2	32	10.9	49.6	15	7.07	185	0.83	16	0.39	3.29	166	2.51	231
G.A.P.24	3.5	146	16.1	109	6.9	3.58	2.25	9.29	1.3	84.1	0.47	43.1	56.4	32	20.4	59.4	17	11.3	218	1.3	21	0.52	3.39	165	3.21	237
G.A.P.25	3.7	125	16.8	118	5.41	3.25	1.37	6.01	1.13	73.4	0.44	43.4	44.7	34	12.3	49.6	17	7.42	201	0.89	18	0.49	3.24	150	2.96	250
G.A.P.26	3.8	169	16.1	114	7.1	3.87	2.03	8.67	1.38	97.9	0.5	43.8	60.7	33	22.9	62.2	20	10.8	221	1.22	34	0.56	3.45	160	3.5	246
G.A.P.27	3.6	105	17.2	112	4.57	2.69	1.19	5.02	0.92	62.2	0.38	43.3	36.6	33	10.2	45.6	17	6.22	195	0.74	15.4	0.41	3.19	170	2.57	235
G.A.P.28	5	164	16.2	135	6.31	3.53	1.7	7.48	1.23	97.3	0.49	45.6	57.7	31	22.3	90.2	28	9.61	228	1.05	33.4	0.53	3.74	203	3.28	247
G.A.P.29	5	170	17.3	127	6.44	3.49	1.86	8.12	1.25	98.5	0.47	44.5	61.6	33	23.5	87.2	24	10.5	199	1.11	32.4	0.52	3.35	179	3.21	233
G.A.P.31	2.8	112	17.1	113	6.68	3.16	2.37	9.52	1.21	64.3	0.41	27.1	49	30	11.9	63.1	20	11.4	166	1.33	16.3	0.45	2.41	155	2.75	190
G.A.P.33	2.6	110	15.9	117	5.87	2.89	2.03	7.89	1.06	62.8	0.37	20.8	45.9	33	11.6	78.6	20	9.85	173	1.11	16.8	0.43	2.66	161	2.63	180
G.A.P.34	3.8	149	17.7	104	6.2	3.48	1.62	6.86	1.21	86.1	0.47	43.6	53.4	33	20.5	57.1	18	8.65	217	0.99	26	0.52	3.4	163	3.18	245
G.A.P.36	3	141	17	119	6.08	3.23	1.9	7.7	1.17	81.2	0.42	35.4	51.4	38	13.9	44.3	18	9.56	232	1.07	21	0.47	3.07	123	2.93	213
G.A.P.37	2.8	141	15.2	110	5.34	3.1	1.53	6.46	1.08	84.7	0.44	38.8	46.4	34	13.2	45.2	18	7.87	225	0.9	34.1	0.47	2.88	129	2.92	244

from 0.05 to 0.15 wt. % (average 0.09) and from 0.01 to 0.05 wt. % (average 0.03), respectively. Major oxides are plotted against Al_2O_3 in Figure 5, Fe_2O_3 and TiO_2 have a positive correlation, whereas the rest of them show negative trends. Moreover, the Gadvan mudrocks were normalized to the UCC (Taylor & McLennan 1985) (Fig. 6A). CaO and Na_2O abundances display marked depletion, and TiO_2, Fe_2O_3, and Al_2O_3 contents are slightly enriched relative to the UCC (Fig. 6A).

Trace element concentrations

In comparison with the UCC, the contents of Rb, Sr, and Ba in the studied samples display marked depletion (average/UCC 0.56, 0.54, 0.24, respectively), and the rest of the large ion lithophile elements (LILE) (Th and U) in the Gadvan mudrocks are relatively similar to the UCC (average/UCC 1.92 and 1.07, respectively) (Fig. 6B). Moreover, high field strength elements (HFSE), such as Zr and Nb are relatively similar to the UCC (average/UCC 1.11 and 1.47, respectively) (Fig. 6B). There is a slight enrichment in the Transition Trace Elements (TTE) Cr and V (average/UCC 3.22 and 2.66, respectively) and the rest of them (Co, Ni and Sc) are almost similar to the UCC (Fig. 6B) in the Gadvan mudrocks.

Rare earth element concentrations

The average of total REE (∑REE) concentrations of the Gadvan sediments is 301.37 ppm (Table 4), and these concentrations vary between 177.99 and 414.69 ppm. There is a significant enrichment in REE values in the studied samples (301.37 ppm) relative to the UCC (148 ppm; Rudnick & Gao 2014). In spite of the differences in abundance, the chondrite normalized REE pattern of samples is similar to the UCC (Fig. 6C), which implies homogenization of these clastic

Table 4: Useful geochemical parameters of the studied samples from the Gadvan Formation.

Sample No.	∑REE	∑LREE	∑HREE	∑LREE/∑HREE	Gd_N/Yb_N	Eu/Eu*	La/Th	La/Sc	La/Sm	Tb/Yb	Th/Yb
G.A.P.2	324.70	300.78	23.92	12.57	1.44	0.64	3.89	3.54	8.57	0.35	6.90
G.A.P.3	270.59	250.76	19.83	12.65	1.21	0.63	3.42	3.56	10.01	0.31	7.44
G.A.P.5	312.07	288.60	23.47	12.30	1.95	0.63	2.48	4.49	7.12	0.45	12.18
G.A.P.7	272.26	252.98	19.28	13.12	1.80	0.66	4.03	2.95	8.13	0.42	7.89
G.A.P.8	266.32	246.82	19.50	12.66	1.45	0.67	3.81	3.41	8.73	0.36	7.30
G.A.P.9	256.37	237.60	18.77	12.66	1.35	0.66	3.76	3.12	8.79	0.34	6.97
G.A.P.10	396.26	344.00	52.26	6.58	3.58	0.71	4.66	3.33	2.75	0.84	4.46
G.A.P.11	229.63	210.10	19.53	10.76	1.20	0.67	4.23	2.69	8.93	0.30	5.28
G.A.P.12	229.18	209.90	19.28	10.89	1.19	0.65	4.19	2.67	8.92	0.30	5.36
G.A.P.13	211.54	194.65	16.89	11.52	1.09	0.65	4.14	2.73	9.98	0.28	5.50
G.A.P.14	177.99	162.77	15.22	10.69	1.01	0.62	4.67	3.01	10.71	0.26	4.62
G.A.P.15	372.12	331.40	40.72	8.14	1.99	0.66	5.29	5.33	5.33	0.50	4.01
G.A.P.16	349.01	320.76	28.25	11.35	1.13	0.63	5.09	5.21	8.98	0.27	4.20
G.A.P.17	238.80	220.74	18.06	12.22	1.30	0.61	4.11	4.09	9.37	0.33	6.42
G.A.P.18	248.76	230.59	18.17	12.69	1.36	0.61	4.12	4.28	9.74	0.33	6.90
G.A.P.19	319.46	295.30	24.16	12.22	1.48	0.64	4.07	4.84	9.04	0.37	6.99
G.A.P.20	343.97	320.31	23.66	13.54	1.31	0.62	2.87	4.42	10.39	0.32	10.20
G.A.P.21	305.97	284.60	21.37	13.32	1.26	0.62	4.06	4.68	10.21	0.31	7.03
G.A.P.22	414.69	375.90	38.79	9.69	2.37	0.66	2.89	4.75	5.76	0.55	9.68
G.A.P.23	254.61	234.87	19.74	11.90	1.34	0.64	4.11	4.38	9.29	0.33	6.37
G.A.P.24	347.02	318.20	28.82	11.04	1.68	0.65	4.00	4.95	7.44	0.40	6.54
G.A.P.25	284.77	262.82	21.95	11.97	1.18	0.61	4.08	4.32	9.89	0.30	6.08
G.A.P.26	390.13	361.30	28.83	12.53	1.43	0.62	2.88	4.90	9.06	0.35	9.71
G.A.P.27	238.71	220.22	18.49	11.91	1.13	0.63	4.04	3.66	10.00	0.29	5.99
G.A.P.28	376.51	350.91	25.60	13.71	1.32	0.59	2.91	3.48	10.12	0.32	10.18
G.A.P.29	390.57	364.10	26.47	13.76	1.46	0.59	3.04	4.10	9.38	0.35	10.09
G.A.P.31	276.48	248.60	27.88	8.92	2.00	0.68	3.94	3.22	5.64	0.48	5.93
G.A.P.33	264.43	240.15	24.28	9.89	1.74	0.68	3.74	3.14	6.38	0.42	6.39
G.A.P.34	342.18	317.65	24.53	12.95	1.25	0.62	3.31	4.78	9.95	0.31	8.18
G.A.P.36	322.03	297.06	24.97	11.90	1.52	0.66	3.87	4.51	8.49	0.37	7.17
G.A.P.37	315.41	293.17	22.24	13.18	1.28	0.64	2.48	4.71	10.76	0.31	11.68
Mean	**301.37**	**277.02**	**24.35**	**11.38**	**1.53**	**0.65**	**3.62**	**3.92**	**7.99**	**0.37**	**7.20**

rocks (LREE enrichment, negative Eu anomaly and nearly flat HREE).

Discussion

Sediment classification and composition

Based on the geochemical classification diagram of Herron (1988; Fig. 7), the studied mudrocks are classified as Fe-shale to shale.

In order to distinguish the different lithologies, Al_2O_3 was chosen as a normalization factor due to its immobile nature during weathering, diagenesis, and metamorphism as well (Bauluz et al. 2000). In general, the negative correlation of major oxides and trace elements (Sr and Ba) with Al_2O_3 is an indicator for the loss of feldspars and removal of soluble elements from the clastic fraction during chemical weathering in the source area (Fig. 6A and B) (Tawfik et al. 2018). Also, a significant negative correlation between SiO_2 and Al_2O_3 (Fig. 5) is evidenced by the sorting effect, as well as hydrodynamic fractionation relative to the UCC (Ramos-Vázquez et al. 2017; Kettanah et al. 2021). The UCC normalized plots demonstrate that some elements are enriched and many are depleted relative to the UCC (Fig. 6A and B). Accordingly, in the Gadvan shales, with regards to the UCC, depletion of SiO_2, and enrichment of Al_2O_3, TiO_2, and Fe_2O_3 are identified. On the other hand, shales are enriched in Fe_2O_3 due to the presence of pyrite in the moldic porosities or replacement of shells. The depletion of Na_2O and K_2O and the $K_2O/Na_2O>1$ can be implied to a relatively smaller amount of Na-rich minerals in them. Low feldspar content is verified by depletion of Ba, Rb, and Sr, which are associated with feldspars (Armstrong-Altrin et al. 2017; Hu et al. 2019; Wang et al. 2019). The terrigenous nature of these shales and high organic matter content are the reasons for the depletion of CaO relative to UCC.

Zr, Sr, V, Rb, La, Cr, Ce, Nb, Pr, and Ni are enriched in the studied samples relative to the UCC. The lower content of Sr relative to the UCC (Fig. 6B) is likely due to the destruction of calcic plagioclase, whereas enrichment of Zr is generally due to the occurrence of zirconium minerals (Hossain 2019; Bessa et al. 2021). Slight enrichment of Nb compared to Zr in the studied samples could be due to the more absorbable nature to clay minerals in mudstones. Higher mean contents of the REE, Zr, Th, Ce, and Y could be the result of relatively higher

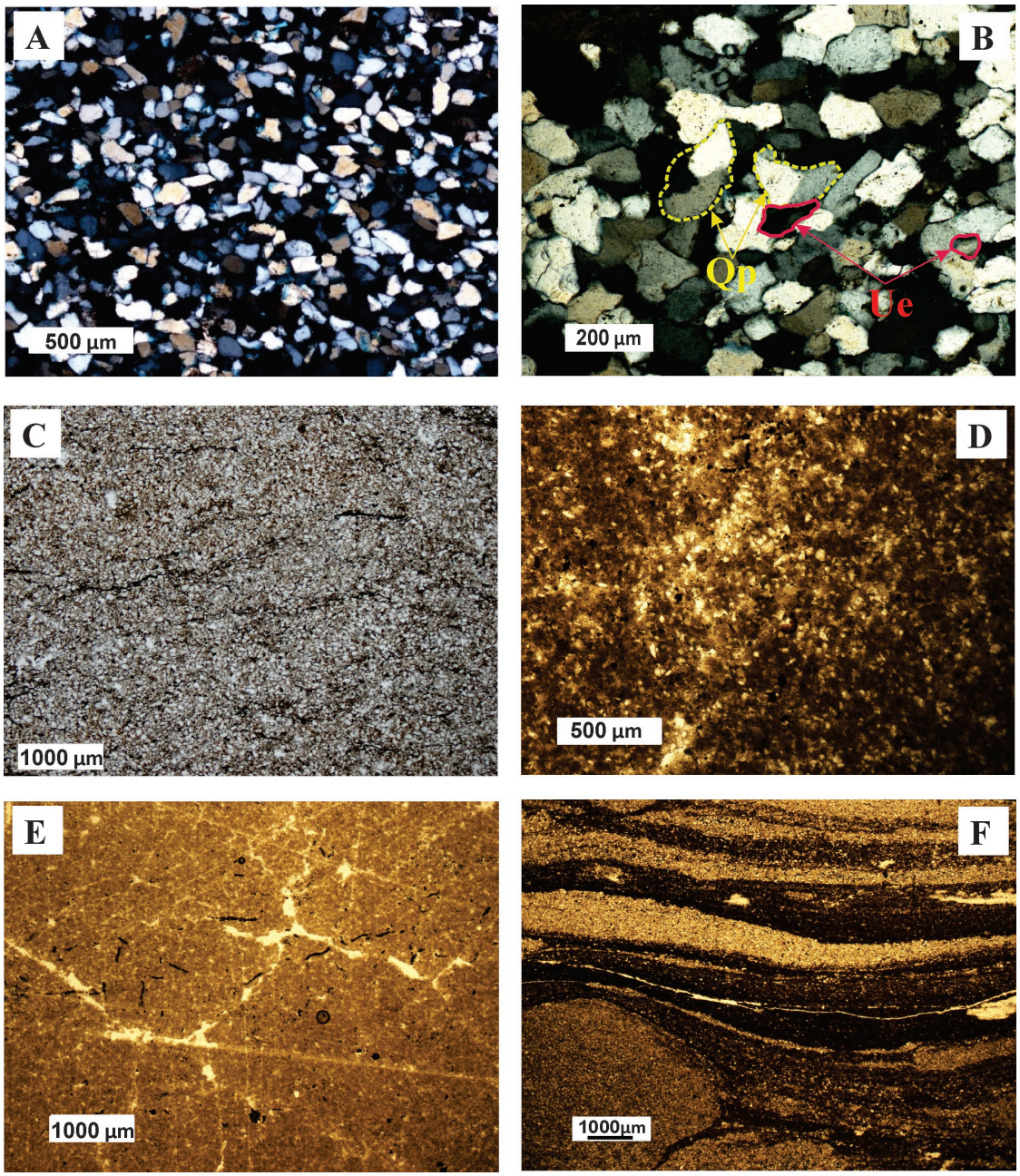

Fig. 3. Photomicrographs of the parent rock's properties evidences and the studied mudrocks. **A** — General view of Gadvan sandstones. **B** — Polycrystalline quartz (Qp) and weakly undulatory (Ue) of monocrystalline quartz. **C** — Siltstone. It can be seen that the Gadvan siltstones have a moderately laminated structure. **D** — Silty mudstone. **E** — Mudstone. Black assemblies are pyrite or residual hydrocarbons. **F** — Laminated shale (dark laminae are enriched in organic matter).

abundances of REE bearing heavy minerals like zircon, monazite, allanite, etc. (McLennan 1989; Ramos-Vázquez et al. 2017). Similarly, enrichment of Nb, Ni, Cr, and V is due to the clay-rich nature of the studied samples relative to UCC (Hossain 2019; Mustafa & Tobia 2020).

Paleoweathering and sediment recycling

As a weathering product, mudrocks contain more clays than sandstones, hence they are highly useful for measuring the intensity of weathering in the source area (Anaya-Gregorio et al. 2018; Hernández-Hinojosa et al. 2018; Ayala-Pérez et al. 2021). Parent rock type and lithology in the source area strongly controls the chemical composition of sediments and weathering intensities (Fedo et al. 1995; Schneider et al. 2016; Ramos-Vázquez & Armstrong-Altrin 2019). The Chemical Index of Alteration ($CIA = 100 \times [Al_2O_3/(Al_2O_3 + CaO^* + Na_2O + K_2O)]$; Nesbitt & Young 1982) (Fig. 8A) and the Plagioclase Index of Alteration ($PIA = 100 \times [(Al_2O_3 - K_2O)/(Al_2O_3 + CaO^* + Na_2O - K_2O)]$; where CaO* is the content of CaO

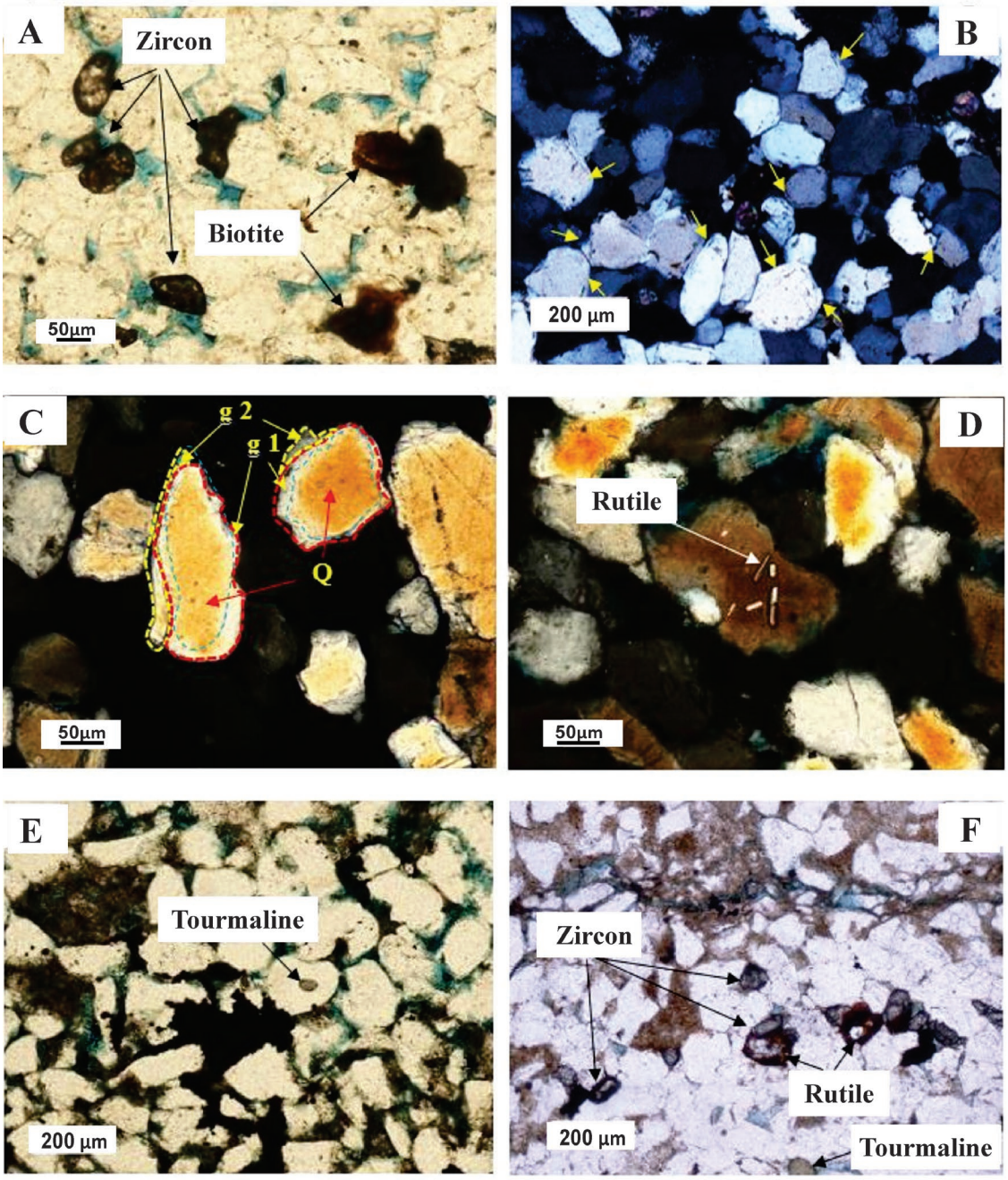

Fig. 4. Photomicrographs of the petrographic evidences of recycling and weathering effects (the vivid colours are due to the thickness of the thin sections). **A** — Rounded zircon and biotite (PPL) in a quartz arenite. **B, C** — Rounded overgrowth and more than one-generation cements (Q=quartz grains and g=generation) (XPL). **D** — Inclusion of rutile needles (XPL) in a quartz grain. **E** — Tourmaline inclusion (PPL) in a quartz grain. **F** — Zircon, rutile and tourmaline in the Gadvan sandstone (PPL).

incorporated in silicate fraction, Fedo et al. 1995) (Fig. 8B) represent the quantitative estimations of secondary clay minerals with respect to the destruction of primary feldspars (Nesbitt & Young 1982; Fedo et al. 1995). The alteration of feldspars increases both values up to 100, while the unweathered rocks have CIA and PIA values near 50 (Nesbitt & Young 1982; Fedo et al. 1995). On the ternary diagrams, the samples plot near to the Al_2O_3 or Al_2O_3–K_2O apex, which is due to the effect of intense weathering in the source area (Fig. 8A and B). The Index of Compositional Variability (ICV $=[(Fe_2O_3+K_2O+Na_2O+CaO+MnO+MgO+TiO_2)/Al_2O_3]$; Cox et al. 1995) (Fig. 8C) is another index for understanding the mineralogical maturity and weathering intensity of sediments. For instance, the main framework minerals have high ICV, whereas clay minerals (kaolinite, illite, and muscovite) have ICV values lower than 0.84 (0.47–0.71, Cox et al. 1995). Samples plotted on the ICV versus CIA diagram imply the intense weathering in the source.

Higher mean contents of the ΣREE could be related to a higher degree of weathering and sedimentary recycling (Shadan & Hosseini-Barzi 2013; Ngueutchoua et al. 2017; Madhavaraju et al. 2021). In the Gadvan sediments, average ΣREE is 301.37, thus suggesting high intensity of weathering. Furthermore, since HREE prefer to retain in solution, another factor which varies due to intense weathering conditions is LREE/HREE (Cantrell & Byrne 1987). The LREE/HREE ratio in the Gadvan mudrocks varies between 6.58 and 13.76, indicating remarkable fractionation, and suggests intense weathering at that time. An increase in the LREE/HREE ratio higher than 4 can be attributed to intense weathering (Vosoughi Moradi et al. 2016). In addition, weathering has a tendency toward oxidation of insoluble U^{4+} to soluble U^{6+}, with loss of solution and elevation of Th/U ratios (McLennan et al. 1980; Somayajulu et al. 1994; Nagarajan et al. 2007, 2011; Armstrong-Altrin 2020). The Th/U ratio of mudrocks from the Gadvan Formation ranges from 3.05 to 12.32, except for one sample, which was less than 4, indicating significant weathering in the source area (Fig. 8D).

The C-value, ∑(Fe+Mn+Cr+Ni+V+Co)/∑(Ca+Mg+Sr+Ba+K+Na), is another indicator successfully applied to infer the paleoclimate of mudrocks (Cao et al. 2012). The mean C-value of the Gadvan mudrocks is 1.7, which reflects a humid or moist paleoclimate in the southwestern parts of the Neo-Tethys during the Early Cretaceous time. The degree of sediment recycling can be inferred by Th/Sc vs. Zr/Sc bivariate plot (McLennan et al. 1993). Th/Sc is an index to determine the provenance, and Zr/Sc is a reliable index to determine the influence of the sedimentary recycling process. On the Th/Sc vs. Zr/Sc diagram, the Gadvan samples plot parallel to trend 2 (sediment recycling – zircon addition), which indicates extreme influence of recycling and compositional variation (Fig. 8E). In the Gadvan mudstones, the variation in Th/Sc (0.64–1.89) and La/Sc (2.67–5.33) ratios (Table 5) is limited, indicating the effect of recycling, which caused variation and homogeneity in the composition of sediments derived from the source and deposited in the Abadan Plain basin.

However, in the Gadvan sandstones, rounded zircon (Fig. 4A), rounded overgrowths (Fig. 4B) and more than 1 generation of overgrowths (Fig. 4C) in some quartz grains, which is the evidence of recycling in the studied samples, indicate a recycling history for most likely quartz rich sedimentary rocks and could be considered a major source rock. Moreover, petrographical evidences, such as predominantly homogeneous, sub-rounded to rounded quartz grains imply the importance of the mechanical effects for rock configuration. Moreover, a lack of unstable grains, such as feldspars and unstable lithic fragments

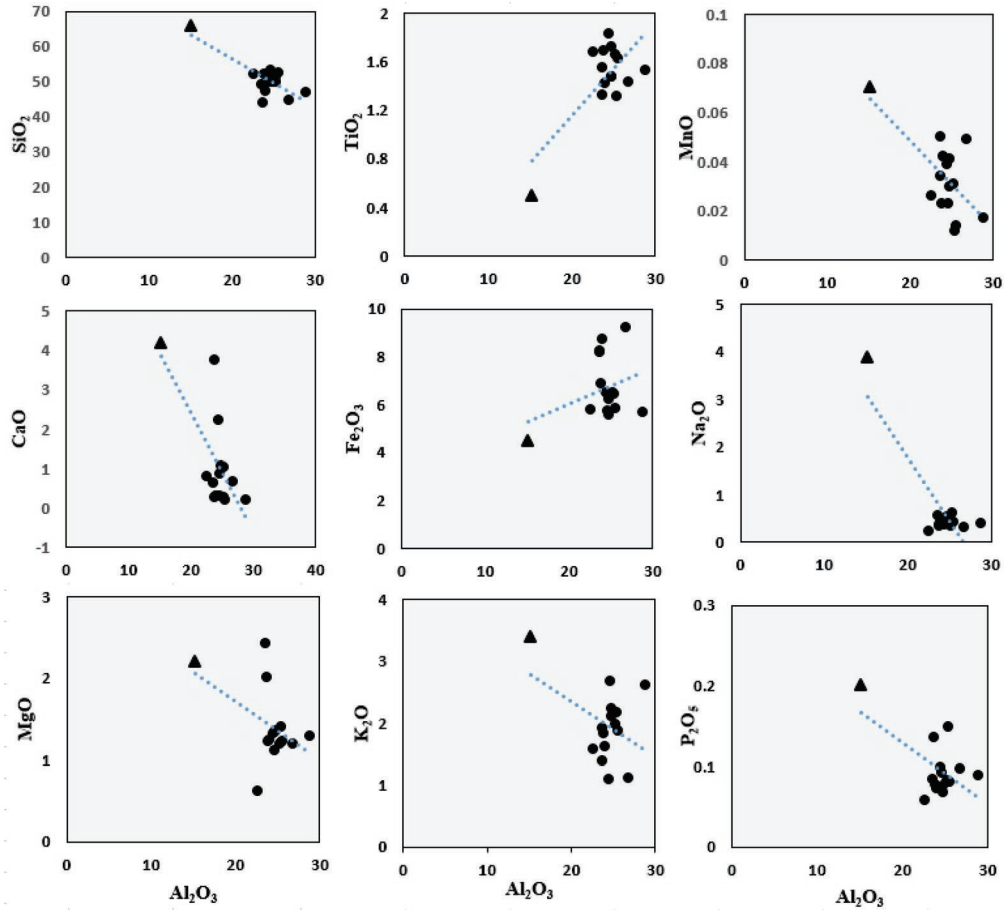

Fig. 5. Graphs of major elements vs. Al_2O_3 showing the distribution of samples from the Gadvan Formation. Triangle is the average of UCC.

could be related to a high degree of chemical weathering. Weathering products of K-feldspar are observed as illite in the mudrock samples (Table 1). These evidences can be due to recycling, long transport, and humid climatic conditions on low relief terrains of the Arabian craton, which is compatible with the Early Cretaceous paleogeographic maps suggested by Scotese (2014). The Abadan Plain was placed near the equator with significant chemico–physical erosional and weathering effective factors.

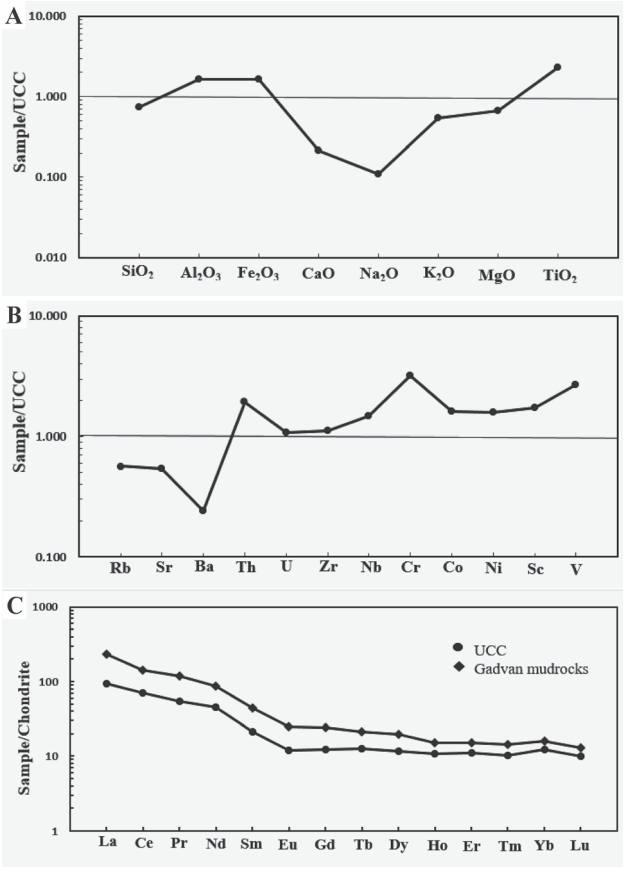

Fig. 6. Spider plots of major oxides (**A**) and trace elements (**B**) of the Gadvan mudrocks, including Large Ion–Lithophile Elements (LILE) (Rb–U), followed by High Field Strength Elements (HFSE) and the Transition Metals (V–Sc) against upper continental crust values from McLennan (2001). **C** — REE chondrite-normalizing factors are from the Gadvan mudrocks and UCC.

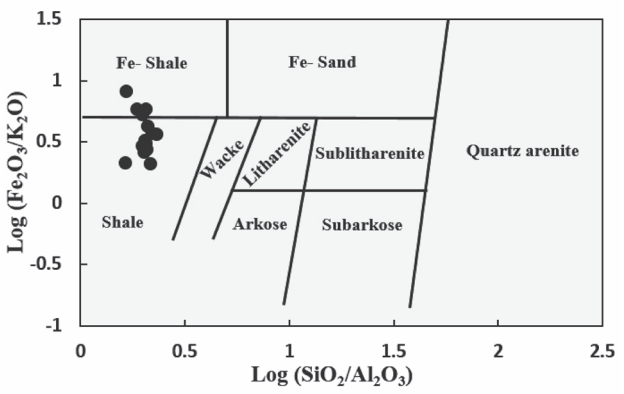

Fig. 7. Geochemical classification diagram (after Herron 1988) for the Gadvan Formation mudrocks.

Source rocks

The low mobility of the few major, trace, and REE of sediments makes them useful indicators to trace sedimentary provenance (Taylor & McLennan 1985; Wronkiewicz & Condie 1987; Roser & Korsch 1988; McLennan et al. 1993; Hayashi et al. 1997; Cullers 2000; Hossain et al. 2010, 2017; Tapia-Fernandez et al. 2017).

The provenance discrimination scheme proposed by Roser & Korsch (1988), based on the abundances of seven major oxides (TiO_2, Al_2O_3, Fe_2O_3, MgO, CaO, Na_2O_3 and K_2O), indicates a progressive loss of feldspar and increase in quartz due to source rock weathering or recycling (Fig. 9A). Among the major oxides, the Al_2O_3/TiO_2 ratio is less affected during weathering, transportation, and diagenesis (Rollinson 1993; Armstrong-Altrin et al. 2015, 2018; Hossain et al. 2018). The Al_2O_3/TiO_2 ratio varies from 3 to 8, ~8 to 21, and ~21 to 70 for mafic, intermediate, and felsic igneous rocks, respectively (Hayashi et al. 1997). In the Gadvan mudrocks, this ratio varies from ~13.35 to 19.26 (average 16.17), and when coupled with moderate to high SiO_2 contents (up to 53 wt. %), their derivation is indicated primarily from intermediate and felsic source materials.

Moreover, slight enrichment of Nb could be interpreted as a signature of the addition of alkaline or continental source rocks (Ravnas & Furnes 1995). Slight enrichment of Cr and Ni suggests that these distributions are likely controlled by phyllosilicate clay minerals and a Cr/Ni ratio between ~2 and 4 (3.57) implies intermediate and/or felsic source rocks. Th and Sc are good indicators of sedimentary provenance because they are quite insoluble, and thus are transported almost exclusively by terrigenous detritus (Potter et al. 2005). Taking into account that felsic rocks are significantly richer in La and Th, as well as poorer in Sc, Cr, and Co than mafic rocks, the La/Sc, La/Co, Th/Sc, and Th/Co ratios are good indicators for source rocks (Taylor & McLennan 1985; Condie 1993; Cullers 1994, 2000; Cullers & Podkovyrov 2000; Armstrong-Altrin et al. 2019, 2021) (Table 5). These ratios in the Gadvan mudrocks are within the range of sediments derived from felsic source rocks, and the mean of these ratios is mostly similar to the upper continental crust composition.

In addition, on the Th/Yb vs. Ta/Yb diagram, the Gadvan samples plot between the continental and fringing arc areas and the average upper continental crust value (Pearce 1983) (Fig. 9B). Furthermore, the La/Sc vs. Co/Th, La/Sc vs. Th/Co, Cr/Th vs. Th/Sc and La/Yb vs. La/Th diagrams reveal felsic and intermediate sources for the Gadvan mudrocks (Condie & Wronkiewicz 1990; Shao et al. 2001; Cullers 2002; Gu et al. 2002) (Fig. 9C, D, E, and F). The Gd_N/Yb_N ratios in the upper crustal rocks vary from 1.0 to 2.0 (McLennan et al. 1993).

The average of Gd_N/Yb_N ratio for the Gadvan sediments is 1.53 (Table 4), indicating either an upper crustal composition or felsic volcanic rock composition. Therefore, on the basis of these results, in addition to the high LREE/HREE ratio, La/Sc, Th/Sc, and Th/Co ratios, as well as the REE and negative Eu anomaly (Eu/Eu^*=0.59–0.71, average=0.65) (Table 4), we can infer a felsic to intermediate continental rock as the source for the Gadvan mudrocks.

The type of extinction, monocrystallinity or polycrystallinity, the type of contact between grains, and the composition

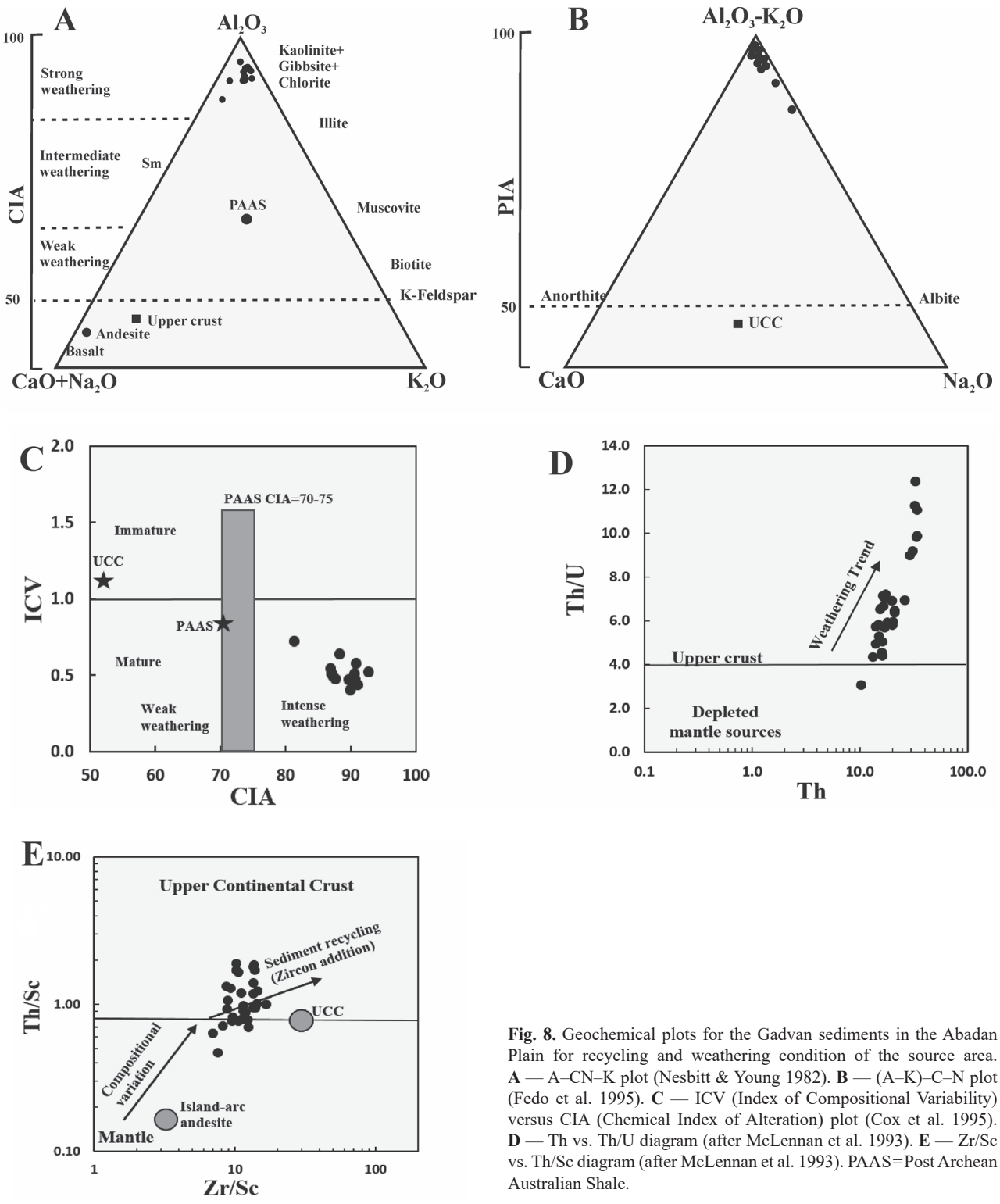

Fig. 8. Geochemical plots for the Gadvan sediments in the Abadan Plain for recycling and weathering condition of the source area. **A** — A–CN–K plot (Nesbitt & Young 1982). **B** — (A–K)–C–N plot (Fedo et al. 1995). **C** — ICV (Index of Compositional Variability) versus CIA (Chemical Index of Alteration) plot (Cox et al. 1995). **D** — Th vs. Th/U diagram (after McLennan et al. 1993). **E** — Zr/Sc vs. Th/Sc diagram (after McLennan et al. 1993). PAAS=Post Archean Australian Shale.

Table 5: Ranges of elemental ratios of shales in this study compared to the ratios in similar fractions derived from felsic and mafic rocks (Cullers 1994, 2000; Cullers & Podkovyrov 2000), upper continental crust (Taylor & McLennan 1985), basalt and andesite (Condie 1993). The data values that are more similar to the Gadvan samples are marked in grey.

Elemental ratio	Gadvan samples[1] Range	Mean	Range of sediment from felsic sources[2]	Range of sediment from mafic sources[2]	Upper continental crust[3]	Andesites[4]	Basalts[4]
La/Sc	2.67–5.33	3.9	2.50–16.3	0.43–0.86	2.21	1.05	0.32
La/Co	2.90–6.71	4.6	1.80–13.8	0.14–0.38	1.76	0.74	0.29
Th/Sc	0.64–1.89	1.08	0.84–20.5	0.05–0.22	0.79	0.17	0.07
Th/Co	0.69–2.69	1.27	0.67–19.4	0.04–1.40	0.63	0.12	0.06

1 – This study; 2 – Cullers 1994, 2000; Cullers & Podkovyrov 2000; 3 – Taylor & McLennan 1985; 4 – Condie 1993.

of grains are some important factors which are considered for study of the parent rocks. In the Gadvan sandstones, undulosity is more usual than polycrystallinity. Moreover, evidences in the Gadvan sandstones, such as higher abundance of undulose monocrystalline quartz than polycrystalline quartz (2–4 grains) (Fig. 3A and B), rutile (Fig. 4D), tourmaline inclusions (Fig. 4E and F), zircon and non-undulatory to slightly undulatory extinction in quartz grains, scarcely biotite and a small orientation of grains could be related to low-grade metamorphism in a felsic plutonic parent rock (e.g., Jafarzadeh & Hosseini-Barzi 2008). According to geochemical and petrographic evidences, the seemingly Late Proterozoic Arabian Shield is an extended massive granitoid in the western part of the studied area and the nearest probable provenance for the Gadvan Formation.

Tectonic setting

On the K_2O/Na_2O vs. SiO_2 diagram, the Gadvan mudrocks plot on the passive margin (PM) field (Fig. 10A; Roser & Korsch 1986). The Th–Sc–Zr/10 and La–Th–Sc triangular diagrams and MMI reveal an active + passive continental margin setting for the Gadvan mudrocks (Fig. 10B and C; Bhatia & Crook 1986). Based on the major element concentrations, Verma & Armstrong-Altrin (2013) proposed a discriminant function diagram to discriminate among island arc or continental arc, continental rift, and continental collision settings (Fig. 10D). For example, active margin includes the sediments derived from arc and collision settings, and the passive margin comprises sediments from the rift setting (Verma & Armstrong-Altrin 2013, 2016). On the discriminant function diagram (Fig. 10B), most of the Gadvan mudrocks plot in the collision field, suggesting that the studied rocks were derived from active continental margin, which is a part of collision or convergence. Therefore, it can be implied that the Gadvan mudrocks were subjected to very complex processes controlled by regional tectonism. In other words, this can be the result of the convergence process between the Arabian and Iranian plates since that time (e.g., LaMaskin et al. 2008; Jafarzadeh et al. 2014; Gazi et al. 2017). Berberian & King (1981) and Davoudzadeh et al. (1981) believed that convergence of these two plates began from the Late Triassic to the Early Jurassic. However, Mohajjel & Fergusson (2000), Hessami et al. (2001), Alavi (2004) and Molinaro et al. (2004) proposed that convergence of the Arabian and Iranian plates started from the Late Jurassic to the Early Cretaceous simultaneously with the deposition of the Gadvan Formation in the south-west of the Neo-Tethys margin. Plotting of the samples in the collision zone, including our new above-mentioned results, proved that the convergence started before the Early Cretaceous.

Conclusion

- The Gadvan sandstones texturally vary from sub-mature to mature, very fine- to fine-grained, and they are classified as quartz arenite. XRD analysis on mudrocks demonstrates that the main constituent minerals comprise quartz, feldspar, calcite, pyrite, kaolinite, illite, and heavy minerals.
- The indices of weathering and alteration (CIA, PIA and ICV) indicate intense weathering in the source area.
- Th/Sc vs. Zr/Sc bivariate plot demonstrates sediment recycling. The variations in Th/Sc and La/Sc ratios are indicative of sedimentary recycling processes.
- The provenance discrimination diagrams and the Al_2O_3/TiO_2 ratio suggest the derivation of the studied sediments from the felsic to intermediate source rocks. Slight enrichment of Nb, Zr, Th, La, Cr and Ni, and Cr/Ni ratios between ~2 and 4, high LREE/HREE ratio (11.38) as well as La/Sc, La/Co, Th/Sc, and Th/Co ratios indicate the alkaline or continental source rocks. In addition, other bivariate diagrams based on trace element concentrations reveal a felsic provenance. The Gadvan sandstones are moderately to well-sorted and rounded to sub-rounded, with abundance of monocrystalline quartz grains and a few feldspars, which can be related to a felsic parent rock. However, greater abundance of weakly, undulose monocrystalline than polycrystalline quartz (2–4 sub-grains), as well as the existence of some mica grains could suggest low-grade metamorphism. The geochemical and petrographical evidences imply a felsic and low-grade metamorphic parent rock, similar to the massive granitoids of the Arabian Shield.
- The discrimination diagrams confirm the active continental margin tectonic setting of the Gadvan sedimentary basin related to the beginning of convergence and the collision process between the Arabian and Iranian plates before the Early Cretaceous.

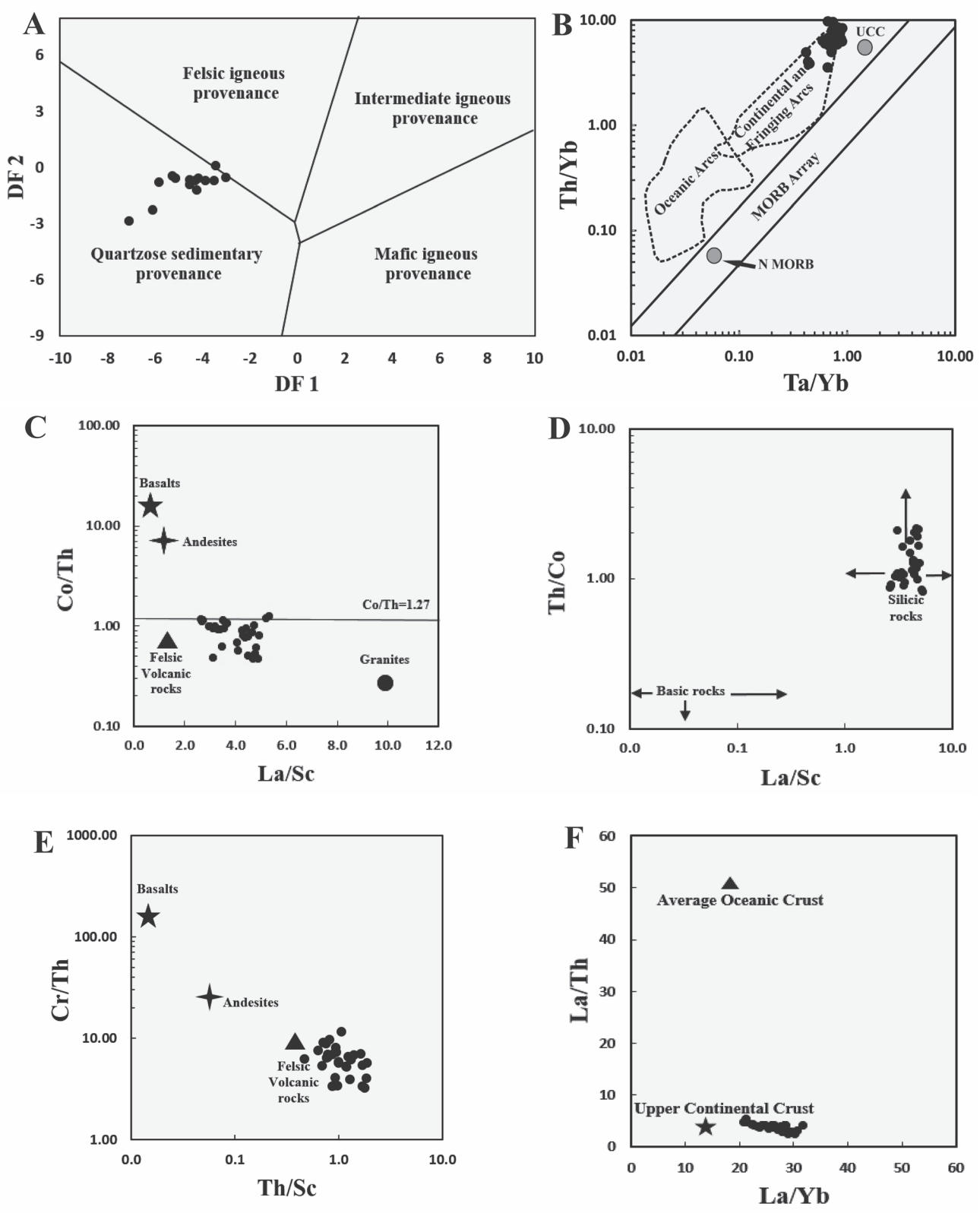

Fig. 9. Source rock composition diagrams based on major oxides and immobile trace elements for the Gadvan sediments in the Abadan Plain. **A** — Major element provenance discriminant plot (Roser & Korsch 1988). **B** — Th/Yb vs. Ta/Yb plot (modified after Pearce 1983). **C** — La/Sc vs. Co/Th plot (Gu et al. 2002). **D** — La/Sc vs. Th/Co plot (after Cullers 2002). **E** — Th/Sc vs. Cr/Th plot (after Condie & Wronkiewicz 1990). **F** — La/Yb vs. La/Th plot (Shao et al. 2001). MORB=Mid-Ocean Ridge Basalt.

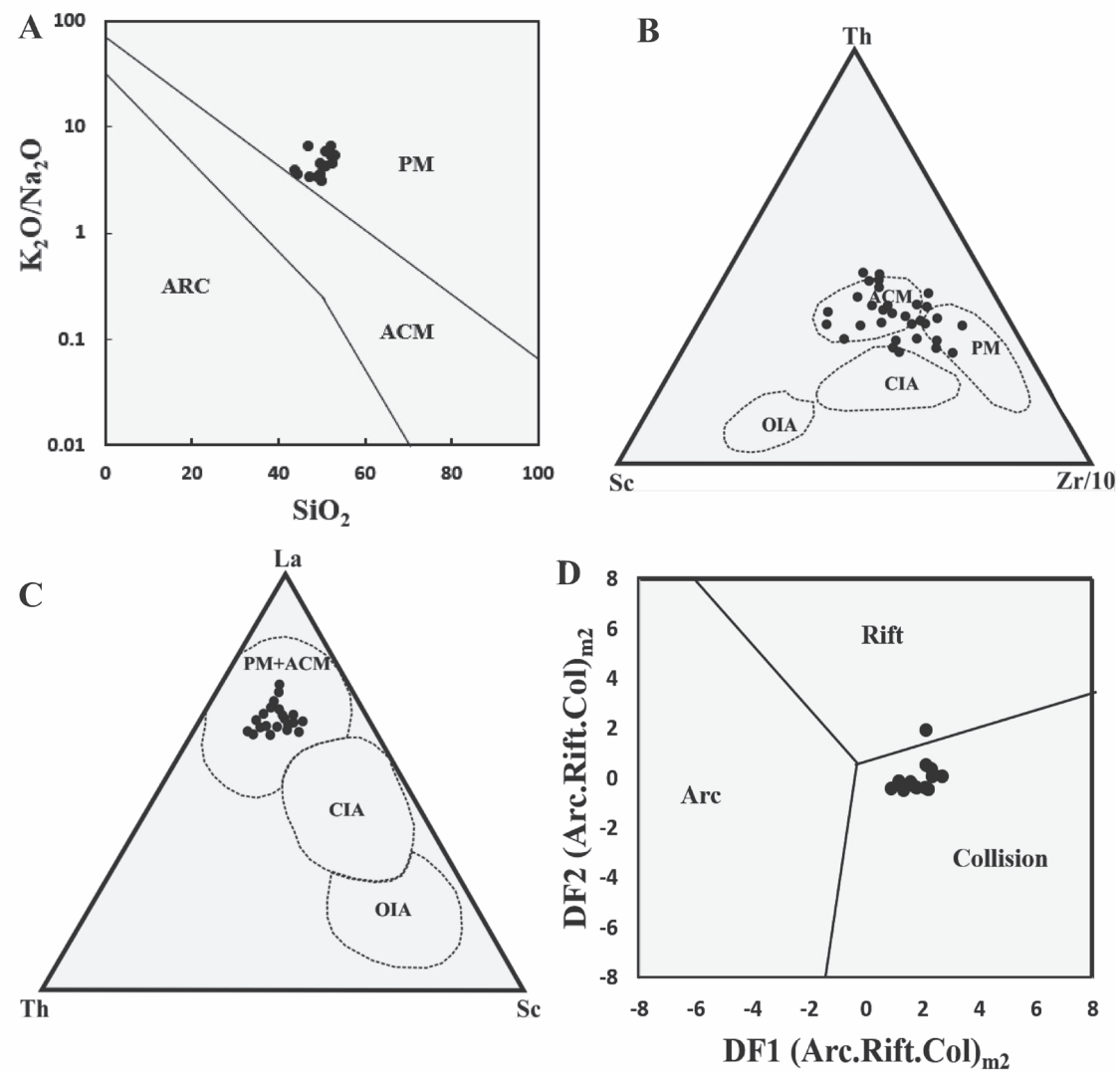

Fig 10. Tectonic setting discrimination diagrams based on major oxides and immobile trace elements for the Gadvan sediments in the Abadan Plain. **A** — SiO_2 vs. Log (K_2O/Na_2O) binary diagram (Roser & Korsch 1986). **B** — Th–Sc–Zr/10 plot (after Bhatia & Crook 1986). **C** — La–Th–Sc plot (from Bhatia & Crook 1986). OIA=Oceanic Island Arc, CIA=Continental Island Arc, PM+ACM=Passive and Active Continental Margin. **D** — DF1 vs DF2 plot (Verma & Armstrong-Altrin 2013).

Acknowledgements: The authors wish to thank the Research Institute of Petroleum Industry (RIPI) for financial support and permission to publish this research. We thank the associate editor, Katarína Bónová, two reviewers (Marek Vďačný and an anonymous reviewer) for their helpful comments and suggestions to improve our final version of the manuscript.

References

Alavi M. 2004: Regional stratigraphy of the Zagros fold-thrust belt of Iran and its proforeland evolution. *American Journal of Science* 304, 1–20. https://doi.org/10.2475/ajs.304.1.1

Alavi M. 2007: Structures of the Zagros fold-thrust belt in Iran. *American Journal of Science* 307, 1064–1095. https://doi.org/10.2475/01.2008.05

Al-Fares A.A., Bouman M. & Jeans P. 1998: A new look at the Middle to Lower Cretaceous stratigraphy, offshore Kuwait. *GeoArabia* 3, 543–560.

Anaya-Gregorio A., Armstrong-Altrin J.S., Machain-Castillo M.L., Montiel-García P.C. & Ramos-Vázquez M.A. 2018: Textural and geochemical characteristics of late Pleistocene to Holocene fine-grained deep-sea sediment cores (GM6 and GM7), recovered from southwestern Gulf of Mexico. *Journal of Paleogeography* 7, 253–271. https://doi.org/10.1186/s42501-018-0005-3

Aqrawi A.A. & Badics B. 2015: Geochemical characterisation, volumetric assessment and shale-oil/gas potential of the Middle Jurassic–Lower Cretaceous source rocks of NE Arabian Plate. *GeoArabia* 20, 99–140.

Armstrong-Altrin J.S. 2015: Evaluation of two multi-dimensional discrimination diagrams from beach and deep sea sediments from the Gulf of Mexico and their application to Precambrian clastic sedimentary rocks. *International Geology Review* 57, 1446–1461. https://doi.org/10.1080/00206814.2014.936055

Armstrong-Altrin J.S. 2020: Detrital zircon U–Pb geochronology and geochemistry of the Riachuelos and Palma Sola beach sediments, Veracruz State, Gulf of Mexico: a new insight on palaeoenvironment. *Journal of Palaeogeography* 9, 28. https://doi.org/10.1186/s42501-020-00075-9

Armstrong-Altrin J.S., Lee Y.I., Verma S.P. & Ramasamy S. 2004: Geochemistry of sandstones from the Upper Miocene Kudankulam Formation, southern India: implications for provenance, weathering, and tectonic setting. *Journal of Sedimentary Research* 74, 285–297. https://doi.org/10.1306/082803740285

Armstrong-Altrin J.S., Lee Y.I., Kasper-Zubillaga J.J., Carranza-Edwards A., Garcia D., Eby G.N., Balaram V. & Cruz-Ortiz N.L. 2012: Geochemistry of beach sands along the western Gulf of Mexico, Mexico: implication for provenance. *Geochemistry* 72, 345–362. https://doi.org/10.1016/j.chemer.2012.07.003

Armstrong-Altrin J.S., Nagarajan R., Lee Y.I., Kasper-Zubillaga J.J. & Córdoba-Saldaña L.P. 2014: Geochemistry of sands along the San Nicolás and San Carlos beaches, Gulf of California, Mexico: implications for provenance and tectonic setting. *Turkish Journal of Earth Sciences* 23, 533–558.

Armstrong-Altrin J.S., Machain-Castillo M.L., Rosales-Hoz L., Carranza-Edwards A., Sanchez-Cabeza J.A. & Ruíz-Fernández A.C. 2015: Provenance and depositional history of continental slope sediments in the Southwestern Gulf of Mexico unraveled by geochemical analysis. *Continental Shelf Research* 95, 15–26. https://doi.org/10.1016/j.csr.2015.01.003

Armstrong-Altrin J.S., Lee Y.I., Kasper-Zubillaga J.J. & Trejo-Ramírez E. 2017: Mineralogy and geochemistry of sands along the Manzanillo and El Carrizal beach areas, southern Mexico: implications for paleoweathering, provenance, and tectonic setting. *Geological Journal* 52, 559–582. https://doi.org/10.1002/gj.2792

Armstrong-Altrin J.S., Ramos-Vázquez M.A., Zavala-León A.C. & Montiel-García P.C. 2018: Provenance discrimination between Atasta and Alvarado beach sands, western Gulf of Mexico, Mexico: Constraints from detrital zircon chemistry and U–Pb geochronology. *Geological Journal* 53, 2824–2848. https://doi.org/10.1002/gj.3122

Armstrong-Altrin J.S., Botello A.V., Villanueva S.F. & Soto L.A. 2019: Geochemistry of surface sediments from the northwestern Gulf of Mexico: implications for provenance and heavy metal contamination. *Geological Quarterly* 63, 522–538. https://doi.org/10.7306/gq.1484

Armstrong-Altrin J.S., Ramos-Vázquez M.A., Hermenegildo-Ruiz N.Y. & Madhavaraju J. 2021: Microtexture and U-Pb geochronology of detrital zircon grains in the Chachalacas beach, Veracruz State, Gulf of Mexico. *Geological Journal* 56, 2418–2438. https://doi.org/10.1002/gj.3984

Assadi A., Honarmand J., Moallemi S.A. & Abdollahie-Fard I. 2016: Depositional environments and sequence stratigraphy of the Sarvak Formation in an oil field in the Abadan Plain, SW Iran. *Facies* 62, 4. https://doi.org/10.1007/s10347-016-0477-5

Ayala-Pérez M.P., Armstrong-Altrin J.S. & Machain-Castillo M.L. 2021: Heavy metal contamination and provenance of sediments recovered at the Grijalva River delta, southern Gulf of Mexico. *Journal of Earth System Science* 130, 88. https://doi.org/10.1007/s12040-021-01570-w

Backman J., Moran K., McInroy D., Mayer L.A. & IODP Expedition 302 Scientists (Editors) 2006: Arctic Coring Expedition (ACEX): Paleoceanographic and tectonic evolution of the central Arctic Ocean. *Integrated Ocean Drilling Program Management International, Inc*, IODP Proceedings 302, *Texas A&M University*, Edinburgh, 1–396. https://doi.org/10.2204/iodp.proc.302.2006

Bauluz B., Mayayo M.J., Fernandez-Nieto C. & Lopez J.M.G. 2000: Geochemistry of Precambrian and Paleozoic siliciclastic rocks from the Iberian Range (NE Spain): implications for source-area weathering, sorting, provenance, and tectonic setting. *Chemical Geology* 168, 135–150. https://doi.org/10.1016/S0009-2541(00)00192-3

Berberian M. & King G.C.P. 1981: Towards a paleogeography and tectonic evolution of Iran. *Canadian Journal of Earth Sciences* 18, 210–265. https://doi.org/10.1139/e81-019

Bessa A.Z.E., Nguetchoua G., Janpou A. K., El-Amier Y.A., Nguetnga O., Kayou U.R., Bisse S. B., Mapuna E.C.N., Armstrong-Altrin J.S. 2021: Heavy metal contamination and its ecological risks in the beach sediments along the Atlantic Ocean (Limbe coastal fringes, Cameroon). *Earth Systems and Environment* 5, 433–444. https://doi.org/10.1007/s41748-020-00167-5

Bhatia M.R. 1985: Composition and classification of Paleozoic flysch mudrocks of eastern Australia: Implications in provenance and tectonic setting interpretation. *Sedimentary Geology* 41, 249–268.

Bhatia M.R. & Crook K.A.W. 1986: Trace element characteristics of graywackes and tectonic setting discrimination of sedimentary basins. *Contributions to Mineralogy and Petrology* 92, 81–193. https://doi.org/10.1007/BF00375292

Boggs Jr. S. 2009: Petrology of sedimentary rocks. *Cambridge University Press,* New York, 1–600.

Cantrell K.J. & Byrne R.H. 1987: Rare earth element complexation by carbonate and oxalate ions. *Geochimica et Cosmochimica Acta* 51, 597–605. https://doi.org/10.1016/0016-7037(87)90072-X

Cao J., Wu M., Chen Y., Hu K., Bian L., Wang L. & Zhang Y. 2012: Trace and rare earth element geochemistry of Jurassic mudstones in the northern Qaidam Basin, northwest China. *Chemie der Erde* 72, 245–252. https://doi.org/10.1016/j.chemer.2011.12.002

Chittleborough D.J. 1991: Indices of weathering for soils and paleosols formed on silicate rocks. *Australian Journal of Earth Sciences* 38, 115–120. https://doi.org/10.1080/08120099108727959

Condie K.C. 1989: Origin of the Earth's crust. *Palaeogeography Palaeoclimatology Palaeoecology* 75, 57–81. https://doi.org/10.1016/0031-0182(89)90184-3

Condie K.C. 1993: Chemical composition and evolution of the upper continental crust: contrasting results from surface samples and shales. *Chemical Geology* 104, 1–37. https://doi.org/10.1016/0009-2541(93)90140-E

Condie K.C. & Wronkiewicz D.J. 1990: The Cr/Th ratio in Precambrian pelites from the Kaapvaal Craton as an index of craton evolution. *Earth and Planetary Science Letters* 97, 256–267. https://doi.org/10.1016/0012-821X(90)90046-Z

Cox R., Lowe D.R. & Cullers R.L. 1995: The influence of sediment recycling and basement composition on evolution of mudrock chemistry in the southwestern United States. *Geochimica et Cosmochimica Acta* 59, 2919–2940. https://doi.org/10.1016/0016-7037(95)00185-9

Cullers R.L. 1994: The controls on the major and trace element variation of shales, siltstones, and sandstones of Pennsylvanian–Permian age from uplifted continental blocks in Colorado to platform sediment in Kansas, USA. *Geochimica et Cosmochimica Acta* 58, 4955–4972. https://doi.org/10.1016/0016-7037(94)90224-0

Cullers R.L. 2000: The geochemistry of shales, siltstones and sandstones of Pennsylvanian-Permian age, Colorado, USA: implications for provenance and metamorphic studies. *Lithos* 51, 181–203. https://doi.org/10.1016/S0024-4937(99)00063-8

Cullers R.L. 2002: Implications of elemental concentrations for provenance, redox conditions, and metamorphic studies of shales and limestones near Pueblo, CO, USA. *Chemical Geology* 191, 305–327.

Cullers R.L. & Podkovyrov V.N. 2000: Geochemistry of the Mesoproterozoic Lakhanda shales in southeastern Yakutia, Russia:

implications for mineralogical and provenance control, and recycling. *Precambrian Research* 104, 77–93. https://doi.org/10.1016/S0301-9268(00)00090-5

Davoudzadeh M., Soffel H. & Schmidt K. 1981: On the rotation of the Central-East-Iran microplate. *Neues Jahrbuch für Geologie und Paläontologie-Monatshefte* 3, 180–192. https://doi.org/10.1127/njgpm/1981/1981/180

Dobrzinski N., Bahlburg H., Strauss H. & Zhang Q.R. 2004: Geochemical climate proxies applied to the Neoproterozoic glacial succession on the Yangtze Platform, South China. In: Jenkins G.S., McMenamin M.A.S., McKay C.P. & Sohl L. (Eds.): The Extreme Proterozoic: Geology, Geochemistry, and Climate. Geophysical Monograph Series 146. *AGU*, Washington, D.C., 13–32. https://doi.org/10.1029/146GM03

Etemad-Saeed N.A., Hosseini-Barzi M. & Armstrong-Altrin J.S. 2011: Petrography and geochemistry of clastic sedimentary rocks as evidences for provenance of the Lower Cambrian Lalun Formation, Posht-e-badam block, Central Iran. *Journal of African Earth Sciences* 61, 142–159. https://doi.org/10.1016/j.jafrearsci.2011.06.003

Etemad-Saeed N., Hosseini-Barzi M., Adabi M.H., Sadeghi A. & Houshmandzadeh A. 2015: Provenance of Neoproterozoic sedimentary basement of northern Iran, Kahar Formation. *Journal of African Earth Sciences* 111, 54–75. https://doi.org/10.1016/j.jafrearsci.2015.07.003

Fedo C.M., Nesbitt H.W. & Young G.M. 1995: Unraveling the effects of potassium metasomatism in sedimentary rocks and paleosols, with implications for paleoweathering conditions and provenance. *Geology* 23, 921–924. https://doi.org/ 10.1130/0091-7613(1995)023<0921:UTEOPM>2.3.CO;2

Folk R., Andrews P. & Lewis D. 1970: Detrital sedimentary rock classification and nomenclature for use in New Zealand. *Journal of Geology and Geophysics* 13, 937–968. https://doi.org/10.1080/00288306.1970.10418211

Gazi M.Y., Kabir S.M.M., Imam M.B., Rahman A. & Islam M.A. 2017: Geochemistry of Neogene mudrocks from Sitakund anticline, Bengal Basin: implications for provenance, weathering, tectonic setting and depositional environment. *Journal of Geoscience and Environment Protection* 5, 147–171.

Getaneh W. 2002: Geochemistry provenance and depositional tectonic setting of the Adigrat Sandstone northern Ethiopia. *Journal of African Earth Sciences* 35, 185–198. https://doi.org/10.1016/S0899-5362(02)00126-4

Gu X.X., Liu J.M., Zheng M.H., Tang J.X., Qi L. 2002: Provenance and tectonic setting of the Proterozoic turbidites in Hunan, South China; geochemical evidence: *Journal of Sedimentary Research* 72, 393–407.

Hardy R. & Tucker M.E. 1988: Techniques in sedimentology. *Blackwell Scientific Publications* 484, 191–228.

Hayashi K.I., Fujisawa H., Holland H.D. & Ohmoto H. 1997: Geochemistry of ~1.9 Ga sedimentary rocks from northeastern Labrador, Canada. *Geochimica et Cosmochimica Acta* 61, 4115–4137. https://doi.org/10.1016/s0016-7037(97)00214-7

Heins W.A. & Kairo S. 2007: Predicting sand character with integrated genetic analysis. In: Sedimentary Provenance and Petrogenesis, Perspectives from Petrography and Geochemistry. *Special Papers of Geological Society of America* 420, 345–379. https://doi.org/10.1130/2006.2420(20)

Hernández-Hinojosa V., Montiel-García P.C., Armstrong-Altrin J.S., Nagarajan R. & Kasper-Zubillaga J.J. 2018: Textural and geochemical characteristics of beach sands along the western Gulf of Mexico, Mexico. *Carpathian Journal of Earth and Environmental Sciences* 13, 161–174.

Herron M.M. 1988: Geochemical classification of terrigenous sands and shales from core or log data. *Journal of Sedimentary Research* 58, 820–829.

Hessami K., Koyi H.A., Talbot C.J., Tabasi H. & Shabanian E. 2001: Progressive unconformities within an evolving foreland fold-thrust belt, Zagros Mountains. *Journal of the Geological Society* 158, 969–981.

Heydari E. 2008: Tectonics versus eustatic control on supersequences of the Zagros Mountains of Iran. *Tectonophysics* 451, 56–70. https://doi.org/10.1016/j.tecto.2007.11.046

Hossain H.M.Z., 2019: Major, trace, and REE geochemistry of the Meghna River sediments, Bangladesh: Constraints on weathering and provenance. *Geological Journal* 55, 3321–3343. https://doi.org/10.1002/gj.3595

Hossain H.M.Z., Roser B.P. & Kimura J.I. 2010: Petrography and whole-rock geochemistry of the Tertiary Sylhet succession, northeastern Bengal Basin, Bangladesh: Provenance and source area weathering. *Sedimentary Geology* 228, 171–183. https://doi.org/10.1016/j.sedgeo.2010.04.009

Hossain H.M.Z., Kawahata H., Roser B.P., Sampei Y., Manaka T. & Otani S. 2017: Geochemical characteristics of modern river sediments in Myanmar and Thailand: implications for provenance and weathering. *Geochemistry* 77, 443–458.

Hossain I., Tsunogae T., Tsutsumi Y. & Takahashi K. 2018: Petrology, geochemistry and LA–ICP–MS U–Pb geochronology of Paleoproterozoic basement rocks in Bangladesh: an evaluation of calc-alkaline magmatism and implication for Columbia supercontinent amalgamation. *Journal of Asian Earth Sciences* 157, 22–39. https://doi.org/10.1016/j.jseaes.2017.09.016

Hu J., Ma Y., Li Z., Wu Y., Gao W., Peng B., Wei X. & Liu D. 2019: Jurassic sediments geochemical constraints on provenance, weathering process, and paleoclimate variation of the north margin of Qaidam Basin, north-eastern Tibetan Plateau. *Geological Journal* 55, 3247–3257. https://doi.org/10.1002/gj.3542

Jafarzadeh M. & Hosseini-Barzi M. 2008: Petrography and geochemistry of Ahwaz Sandstone Member of Asmari Formation, Zagros, Iran: implications on provenance and tectonic setting. *Revista mexicana de ciencias geológicas* 25, 247–260.

Jafarzadeh M., Harami R.M., Amini A., Mahboubi A. & Farzaneh F. 2014: Geochemical constraints on the provenance of Oligocene–Miocene siliciclastic deposits (Zivah Formation) of NW Iran: implications for the tectonic evolution of the Caucasus. *Arabian Journal of Geosciences* 7, 4245–4263. https://doi.org/10.7306/gq.1433

Kettanah Y.A., Armstrong-Altrin J.S. & Mohammad F.A. 2021: Petrography and geochemistry of siliciclastic rocks of the Middle Eocene Gercus Formation, northern Iraq: Implications for provenance and tectonic setting. *Geological Journal.* https://doi.org/10.1002/gj.3880

Khazaei E., Mahmoudy-Gharaie M.H., Mahboubi A., Moussavi-Harami R. & Taheri J. 2018: Petrography, major and trace elemental geochemistry of the Ordovician-Silurian siliciclastics in north of Tabas Block, Central Iran: Implications for provenance and paleogeography. *Journal of Sciences, Islamic Republic of Iran* 29, 129–142. https://doi.org/10.22059/JSCIENCES.2018.65019

Kunze G.W. & Dixon J. 1986: Pretreatment for mineralogical analysis. Methods of Soil Analysis: Part 1. *Physical and Mineralogical Methods* 5, 91–100. https://doi.org/10.2136/sssabookser5.1.2ed.c5

LaMaskin T.A., Dorsey R.J. & Vervoort J.D. 2008: Tectonic controls on mudrock geochemisry, Mesozoic rocks of eastern Oregon and western Idaho, USA: Implications for cordilleran tectonics. *Journal of Sedimentary Research* 7812, 765–783. https://doi.org/10.2110/jsr.2008.087

Loosveld R.J., Bell A. & Terken J.J. 1996: The tectonic evolution of interior Oman. *GeoArabia* 1, 28–51.

Madhavaraju J., Armstrong-Altrin J.S., Pillai R.B. & Pi-Puig T. 2021: Geochemistry of sands from the Huatabampo and Altata bea-

ches. Gulf of California, Mexico. *Geological Journal,* 56, 2398–2417. https://doi.org/10.1002/gj.3864

McLennan S.M. 1989: Rare Earth Elements in Sedimentary Rocks: Influence of Provenance and Sedimentary Processes. *Mineralogical Society of America Reviews in Mineralogy* 21, 169–200.

McLennan S.M. 2001: Relationships between the Trace Element Composition of Sedimentary Rocks and Upper Continental Crust. *Geochemistry, Geophysics, Geosystems* 2. https://doi.org/10.1029/2000GC000109

McLennan S.M., Nance W.B. & Taylor S.R. 1980: Rare earth element – thorium correlations in sedimentary rocks, and the composition of the continental crust. *Geochimica et Cosmochimica Acta* 44, 1833–1839. https://doi.org/10.1016/0016-7037(80)90232-X

McLennan S.M., Hemming S., McDaniel D.K. & Hanson G.N. 1993: Geochemical Approaches to Sedimentation, Provenance and Tectonics. In: Johnsson M.J. & Basu A. (Eds.): Processes Controlling the Composition of Clastic Sediments. *Special Papers of the Geological Society of America* 285, 21–40. https://doi.org/10.1130/SPE284-p21

McQuarrie N. 2004: Crustal scale geometry of the Zagros fold-thrust belt, Iran. *Journal of Structural Geology* 26, 519–535. https://doi.org/10.1016/j.jsg.2003.08.009

Mir A.R. 2015: Rare earth element geochemistry of Post-to Neoarchean shales from Singhbhum mobile belt, Eastern India: implications for tectonic setting and paleo-oxidation conditions. *Chinese Journal of Geochemistry* 34, 401–409.

Mir A.R., Balaram V., Ganai J.A., Dar S.A. & Krishna A.K. 2016: Geochemistry of sedimentary rocks from Permian–Triassic boundary sections of Tethys Himalaya: implications for paleoweathering, provenance, and tectonic setting. *Acta Geochimica* 35, 428–436.

Mohajjel M. & Fergusson C.L. 2000: Dextral transpression in Late Cretaceous continental collision, Sanandaj-Sirjan Zone, western Iran. *Journal of Structural Geology* 22, 1125–1139. https://doi.org/10.1016/S0191-8141(00)00023-7

Molinaro M., Guezou J.C., Leturmy P., Eshraghi S.A. & de Lamotte D.F. 2004: The origin of changes in structural style across the Bandar Abbas syntaxis, SE Zagros (Iran). *Marine and Petroleum Geology* 21, 735–752. https://doi.org/10.1016/j.marpetgeo.2004.04.001

Motiei H. 1993: Geology of Iran: stratigraphy of Zagros. *Geological Survey of Iran*, Tehran, 1–536.

Mustafa R.K. & Tobia F.H. 2020: Geochemical application in unraveling paleoweathering, provenance and environmental setting of the shale from Chia Gara Formation, Kurdistan Region, Iraq. *Iraqi Geological Journal* 53, 90–116.

Nagarajan R., Madhavaraju J., Nagendra R., Armstrong-Altrin J.S. & Moutte J. 2007: Geochemistry of Neoproterozoic shales of the Rabanpalli Formation, Bhima Basin, Northern Karnataka, southern India: implications for provenance and paleoredox conditions. *Revista Mexicana de Ciencias Geológicas* 24, 150–160.

Nagarajan R., Madhavaraju J., Armstrong-Altrin J.S. & Nagendra R. 2011: Geochemistry of Neoproterozoic limestones of the Shahabad formation, Bhima basin, Karnataka, southern India. *Geosciences Journal* 15, 9–25. https://doi.org/10.1007/s12303-011-0005-0

Nath B.N., Plüger W.L. & Roelandts I. 1997: Geochemical constraints on the hydrothermal origin of ferromanganese encrustations from the Rodriguez Triple Junction, Indian Ocean. *Geological Society*, *London, Special Publications* 119, 199–211.

Nesbitt H.W. & Young G.M. 1982: Early Proterozoic climates and plate motions inferred from major element chemistry of lutites. *Nature* 299, 715–717. https://doi.org/10.1038/299715a0

Ngueutchoua G., Ngantchu L.D., Youbi M., Ngos III S., Beyala V.K.K., Yifomju K.P. & Tchamgoué J.C. 2017: Geochemistry of Cretaceous mudrocks and sandstones from Douala Sub-Basin, Kumba Area, South West Cameroon: constraints on provenance, source rock weathering, paleo-oxidation conditions and tectonic environment. *International Journal of Geosciences* 8, 393–424. https://doi.org/10.4236/ijg.2017.84021

Pearce J.A. 1983: Role of the sub-continental lithosphere in magma genesis at active continental margins. In: Hawkesworth C.J. & Norry M.J. (Eds.): Continental basalts and mantle xenoliths, Nantwich, Cheshire. *Shiva Publications*, 230–249.

Pettijohn F.J. 1975: Sedimentary Rocks. 2nd Edition, *Harper and Row Publishers*, New York, 1–628.

Piryaei A., Reijmer J.J.G., van Buchem F.S., Yazdi-Moghadam M., Sadouni J. & Danelian T. 2010: The influence of Late Cretaceous tectonic processes on sedimentation patterns along the northeastern Arabian plate margin (Fars Province, SW Iran). *Geological Society*, *London, Special Publications* 330, 211–251. https://doi.org/10.1016/j.jsg.2019.04.006

Piryaei A., Reijmer J.J.G., Borgomano J. & Van Buchem F.S., 2011: Late Cretaceous tectonic and sedimentary evolution of the Bandar Abbas area, Fars region, southern Iran. *Journal of Petroleum Geology* 34, 157–180. https://doi.org/10.1111/j.1747-5457.2011.00499.x

Potter P.E., Maynard J.B. & Depetris P.J. 2005: Mud and mudstones: Introduction and overview. *Springer-Verlag*, Berlin, 1–297.

Ramos-Vázquez M.A. & Armstrong-Altrin J.S. 2019: Sediment chemistry and detrital zircon record in the Bosque and Paseo del Mar coastal areas from the southwestern Gulf of Mexico. *Marine and Petroleum Geology* 110, 650–675. https://doi.org/10.1016/j.marpetgeo.2019.07.032

Ramos-Vázquez M.A., Armstrong-Altrin J.S., Rosales-Hoz L., Machain-Castillo M.L. & Carranza-Edwards A. 2017: Geochemistry of deep-sea sediments in two cores retrieved at the mouth of the Coatzacoalcos River delta, western Gulf of Mexico, Mexico. *Arabian Journal of Geosciences* 10, 148.

Ravnas R. & Furnes H. 1995: The use of geochemical data in determining the provenance and tectonic setting of ancient sedimentary successions: the Kalvag Melange, western Norwegian Caledonides. In: Plint A.G. (Ed.): Sedimentary Facies Analysis: a Tribute to the Research and Teaching of Harold G. Reading. *Special Publication of the International Association of Sedimentologists* 22, 237–264.

Rollinson H.R. 1993: Using geochemical data: evaluation. Presentation, Interpretation. *Longman Scientific & Technical*, United Kingdom, 1–352.

Roser B.P. & Korsch R.J. 1986: Determination of tectonic setting of sandstone-mudstone suites using SiO_2 content and K_2O/Na_2O ratio. *Journal of Geology* 94, 635–650. https://doi.org/10.1086/629071

Roser B.P. & Korsch R.J. 1988: Provenance signatures of sandstone-mudstone suites determined using discriminant function analysis of major-element data. *Chemical Geology* 67, 119–139. https://doi.org/10.1016/0009-2541(88)90010-1

Rudnick R.L. & Gao S. 2014: Composition of the Continental Crust. *Treatise on Geochemistry* 4, 1–15.

Schneider S., Hornung J., Hinderer M. & Garzanti E. 2016: Petrography and geochemistry of modern river sediments in an equatorial environment (Rwenzori Mountains and Albertine rift, Uganda) – Implications for weathering and provenance. *Sedimentary Geology* 336, 106–119. https://doi.org/10.1016/j.sedgeo.2016.02.006

Scotese C.R. 2014: Atlas of Early Cretaceous paleogeographic maps. PALEOMAP Atlas for ArcGIS, 2, The Cretaceous, Maps 23–31, Mollweide Projection. *PALEOMAP Project*, Evanston, IL.

Sepehr M. & Cosgrove J.W. 2004: Structural framework of the Zagros fold-thrust belt, Iran. *Marine and Petroleum Geology* 21, 829–843. https://doi.org/10.1016/j.marpetgeo.2003.07.006

Shadan M. & Hosseini-Barzi M. 2013: Petrography and geochemistry of the Ab-e-Haji Formation in central Iran: implications for provenance and tectonic setting in the southern part of the Tabas block. *Revista Mexicana de Ciencias Geológicas* 30, 80–95.

Shao L., Stattegger K. & Garbe-Schoenberg C.D. 2001: Sandstone petrology and geochemistry of the Turpan basin (NW China): implications for the tectonic evolution of a continental basin. *Journal of Sedimentary Research* 71, 37–49. https://doi.org/10.1306/041800710037

Sharland P.R., Archer R., Casey D.M., Davies R.B., Hall S.H., Heward A.P., Horbury A.D. & Simmons M.D. 2001: Sequence stratigraphy of the Arabian Plate. *GeoArabia Special Publication* 2, 1–371.

Somayajulu B.L.K., Yadav D.N. & Sarin M.M. 1994: Recent sedimentary records from the Arabian Sea. *Proceedings of the Indian Academy of Sciences – Earth and Planetary Sciences* 103, 315–327. https://doi.org/10.1007/BF02839541

Tapia-Fernandez H.J., Armstrong-Altrin J.S. & Selvaraj K. 2017: Geochemistry and U–Pb geochronology of detrital zircons in the Brujas beach sands, Campeche, Southwestern Gulf of Mexico, Mexico. *Journal of South American Earth Sciences* 76, 346–361. https://doi.org/10.1016/j.jsames.2017.04.003

Tawfik H.A., Salah M.K., Maejima W., Armstrong-Altrin J.S., Abdel-Hameed A.M.T. & Ghandour M.M.E. 2018: Petrography and geochemistry of the Lower Miocene Moghra sandstones, Qattara Depression, north Western Desert, Egypt. *Geological Journal* 53, 1938–1953. https://doi.org/10.1002/gj.3025

Taylor S.R. & McLennan S.M. 1985: The continental crust: its composition and evolution. *Scientific Publications*, Oxford, 1–312.

Tucker M. 1988: Techniques in Sedimentology. *Blackwell*, Oxford, 1–228.

Verma S.P. & Armstrong-Altrin J.S. 2013: New multi-dimensional diagrams for tectonic discrimination of siliciclastic sediments and their application to Precambrian basins. *Chemical Geology* 355, 117–133.

Verma S.P. & Armstrong-Altrin J.S. 2016: Geochemical discrimination of siliciclastic sediments from active and passive margin settings. *Sedimentary Geology* 332, 1–12. https://doi.org/10.1016/j.sedgeo.2015.11.011

Vosoughi Moradi A., Sarı A. & Akkaya P. 2016: Geochemistry of the Miocene oil shale (Hançili Formation) in the Çankırı-Çorum Basin, Central Turkey: Implications for Paleoclimate conditions, source-area weathering, provenance and tectonic setting. *Sedimentary Geology* 341, 289–303. https://doi.org/10.1016/j.sedgeo.2016.05.002

Wang J., He Z., Zhu D. & Ding Q. 2019: Geochemical characteristics, depositional environment, and provenance attitude of the Middle Jurassic Yangye Formation lacustrine mudstones in Kashi Sag, south-western Tarim Basin. *Geological Journal* 55, 2976–2994. https://doi.org/10.1002/gj.3556

Wronkiewicz D.J. & Condie K.C. 1987: Geochemistry of Archean shales from the Witwatersrand Supergroup, South Africa: source-area weathering and provenance. *Geochimica et Cosmochimica Acta* 51, 2401–2416. https://doi.org/10.1016/0016-7037(87)90293-6

Zimmermann U. & Bahlburg H. 2003: Provenance analysis and tectonic setting of the Ordovician clastic deposits in the southern Puna Basin, NW. Argentina. *Sedimentology* 50, 1079–1104. https://doi.org/10.1046/j.1365-3091.2003.00595.x